JNC TN9400 2001-053

MSV : Multi-Scale Viscosity Model of Turbulence
(Research Report)

April, 2001

Japan Nuclear Cycle Development Institute
O-arai Engineering Center

Ⓐ

JNC TN9400 2001-053
April, 2 0 0 1

MSV: MULTI-SCALE VISCOSITY MODEL OF TURBULENCE

Vladimir Kriventsev*

ABSTRACT

Multi-Scale Viscosity (MSV) model is proposed for estimation of the Reynolds stresses in turbulent fully-developed flow in a wall-bounded straight channel of an arbitrary shape.

We assume that flow in an "ideal" channel is always stable, i.e. laminar, but turbulence is developing process of external perturbations cased by wall roughness and other factors. We also assume that real flows are always affected by perturbations of any scale lower than the size of the channel. The turbulence can be modeled in form of internal or "turbulent" viscosity increase.

The main idea of MSV can be expressed in the following phenomenological rule: A local deformation of axial velocity can generate the turbulence with the intensity that keeps the value of local turbulent Reynolds number below some critical value. Here, local turbulent Reynolds number can be defined in two different ways:

i) as a product of value of axial velocity deformation for a given scale and generic length of this scale divided by accumulated value of laminar and turbulent viscosity of lower scales

ii) as a ratio of the difference between total kinetic energy and "flat-profile" kinetic energy to the work of friction forces

In MSV, the only empirical parameter is the critical Reynolds number that is estimated to be around 100 in the former case and about 8.33 in the later.

MSV model has been applied to the fully-developed turbulent flows in straight channels such as a circular tube and annular channel. Friction factor and velocity profiles predicted with MSV are in a good agreement with numerous experimental data.

The MSV model can be classified as "zero-order" integral model of turbulence. Because of simplicity, MSV can be easily implemented for calculation of fully-developed turbulent flows in straight channels of arbitrary shapes including fuel assemblies of nuclear reactors.

The intent of this report is to summarize the progress made in the development of the model of turbulence. Since the final formulations of MSV have not been yet derived, this report should be considered to be preliminary.

---

*) JNC International Fellow

Thermal Hydraulics Research Group, System Engineering Technology Division, O-arai Engineering Center, JNC, Japan

JNC TN9400 2001-053
2 0 0 1 年 4 月

MSV: 乱流の多重スケール粘性モデル

MSV: Multi-Scale Viscosity Model of Turbulence

(研究報告)

Vladimir Kriventsev*

要旨

本研究では、任意形状の壁境界直管流路の完全発達乱流におけるレイノルズ応力を評価できる、多重スケール粘性(MSV) モデルを提案した。

“理想的な” 流路内部の流れは常に安定すなわち層流であるが、壁の表面粗さなどによる外部擾乱のため乱れが発達している流れを仮定する。実際の流れは、流路の寸法より小さいあらゆるスケールの擾乱により常に影響されていると仮定する。乱れは内部の粘性つまり “乱流” 粘性を用いてモデル化できる。

MSV モデルの着想は、以下の現象論的規則により表される：軸方向流速の方向が変わることにより乱れを生じるが、その強さは局所乱流レイノルズ数をある限界値以下に維持するレベルである。すると、局所乱流レイノルズ数の二種類の定義が可能である：

i) 軸方向流速のあるスケールのひずみとこのスケール長さをそれより小さいスケールに対する層流と乱流粘性の和で割った一般的なスケール長さで割った量の積

ii) 一様流速プロファイルの全運動エネルギーと摩擦力による仕事の比

MSV モデルでは、経験定数は限界レイノルズ数のみであり、それは前者の定義では 100 程度、後者の定義では約 8.33 である。

MSV モデルを円管や環状管のような直管の完全発達乱流に適用した。MSV により評価した摩擦係数と速度分布は多くの実験データと良く一致した。

MSV モデルは乱流のゼロ次統合モデルと分類される。従って単純であり、原子炉燃料集合体などの任意形状管路内部の完全発達乱流の計算に容易に適用できる。

本報告書は、MSV 乱流モデルの開発状況をまとめたものである。今後さらに検討を重ねた上で、MSV の定式化を完成させる計画である。

*大洗工学センター　要素技術開発部　流体計算工学研究グループ、国際特別研究員

CONTENTS

LIST OF FIGURES

1. INTRODUCTION

Turbulent flow motions occur in many engineering problems and proper simulation of turbulent flow heat transfer plays an important part in design of nuclear reactor and its components on the "feasibility study" phase. Also, accurate and fast numerical prediction of velocity and temperature filed are very important in safety and accident analysis.

The present sate of turbulence nature understanding is that Navier-Stokes equations can properly describe the turbulent flow. However, direct numerical solution of Navier-Stocks equations is not only too costly but also yet impossible in most important cases for not-very-low Reynolds numbers even in simplest geometries. Instead, averaged Navier-Stokes, or Reynolds equations are considered to be sufficient and practical enough to describe the turbulent flow in most practical applications. Reynolds equations include cross-correlation terms to be estimated with a turbulence model. Such a model should include expressions or/and equations for eddy diffusivity or (in other terms) turbulence viscosity. In this work, we will concentrate on turbulent viscosity modeling of fully-developed wall-bounded incompressible channel flows and propose our original model.

1.1 Turbulence Modeling

One of the first and very effective turbulent viscosity models was a "mixing-length" model proposed by Prandtl [1] long time ago. Prandtl's hypothesis is that fluid particle, or eddy, keeps its axial momentum when moving athwart the flow for some finite distance called "mixing length". According to the mixing length model, turbulent shear stress in athwart direction can be estimated as

$$\tau_{turb} = -\rho\langle u'\upsilon'\rangle = -\rho l^2 \left|\frac{d\langle u\rangle}{dy}\right| \frac{d\langle u\rangle}{dy}, \tag{1}$$

where l is "mixing length"; ρ is density; $u = \langle u\rangle + u'$ and $\upsilon = \langle \upsilon\rangle + \upsilon'$ are axial and cross velocities; y is distance to the wall; index $'$ is devoted for pulsation component of value; and values in brackets $\langle\rangle$ are ensemble averaged. Using the idea Boussinesq's eddy viscosity model, one can write the following expression for eddy diffusivity in athwart direction:

$$\nu_t = -\langle u'\upsilon'\rangle \Big/ \frac{d\langle u\rangle}{dy} = -l^2 \left|\frac{d\langle u\rangle}{dy}\right|, \tag{2}$$

Here, in Eq. (2), the mixing length l should be modeled and Prandtl proposed the following simple relation for pipe flow:

$$l = \chi y, \tag{3}$$

where χ is von Karman constant.

Since only simple formulas (2) and (3) are used here, the Prandtl's mixing length model can be classified as "zero-equation" model in contrast to more complicated modeling that uses additional equations in partial-derivatives derived for other turbulent parameters such as kinetic energy of turbulent fluctuations, dissipation and so on. Zero-equation models were popular because they are relatively simple and intuitive. However, these models are very limited because the can be

applied to particular problems with similar geometry and are inappropriate for predicting other types of flows in more complicated geometries. For example, from Eq. (2) one can easy conclude that turbulent transport becomes exactly zero at the flow symmetry line where axial velocity gradient is zero by definition. While this conclusion opposes the physical phenomenon of turbulence, it does not contribute a lot to the error of calculation simply because the turbulent transport near symmetry line is not very important in most practical cases.

From the middle of twentieth century, with the advance of computer technique, turbulence modeling also advanced. Turbulence modeling in engineering practice progressed to the second-order turbulence closure models in which the second-order turbulence transport quantities are modeled. Comprehensive review of second-order turbulent models can be found in [2]. Although complicated and tedious, these models are considered to be potentially more useful and less problem dependent. However, the latest modifications have proven to be also very dependent on the flow geometry and regimen. For example, four coefficients used in famous k-ε model must be adjusted to different problems to predict relatively accurate solution. Yet k-ε model cannot even predict non-symmetry in eddy-diffusivity distribution for annular channels.

Another alternative is direct numerical simulation (DNS) of Navier-Stokes that becomes more and more popular as computer power grows. Yet, "true" direct simulation is limited by very low Reynolds numbers and no significant achievements can be expected in forecastable future. The promising developing of DNS is its combination with algebraic or second-order modeling to resolve turbulent modes lower than finest mesh size. The resulting model called Large-Eddy Simulation (LES) became very popular in recent years. LES has been applied to many engineering problems including nuclear engineering [3]. However, since LES uses some kind of empirical model of turbulence it cannot be considered as universal. Moreover, LES must always be applied in three dimensions that results in huge demand for computer power.

Long history of "zero-equation" models has proven they posses the advantage of simplicity and are capable of modeling turbulence in many cases. The feeling of the author is that simple zero-order models like Prandtl's mixing length should be applied as a first estimation first to the every new flow in complicated geometry. Also, it seems to be very interesting and promising to enhance a zero-equation modeling using more physical approaches. Thus, the main weakness of mixing-length model is that mixing length itself and turbulence viscosity at a local point are considered to be exactly defined by velocity gradient in this point. However, it's obvious that turbulence parameters must depend on velocity distribution and, perhaps, turbulence intensity relatively far from any given location or, at least, nearby. Second-order modeling resolves this by introducing additional differential equations for energy of turbulence fluctuation, dissipation, and some other virtual variables. However, another approach could be also applied. In 1962, N. Buleev proposed an *integral* model of turbulence based on the consideration of original Prandtl's hypothesis of momentum transported by stochastic eddy movements [4]. Buleev's model results in the system of non-linear integral-differential equations for tensor of turbulent viscosity that can be solved numerically. In spite the fact that Buleev's model could give quite accurate prediction of velocity distribution in very complicated three-dimensional areas such as hexagonal rod bundle array [5], it has been never accepted broadly. It poses some additional calculation complications and, after all, also depends very much on some empirical constants. Here, we recall the Buleev's model because Multi-Scale Viscosity (MSV) proposed in this work can be also categorized as an integral zero-equation model. In fact, MSV is a further development and generalization of Prandtl's and Bullev's mixing length hypothesis.

Before we discuss definitions and assumptions of MSV, let us make some physical considerations related mainly to wall-bounded channel flows.

1.2 Reynolds Number and Transition to Turbulence

The first systematic investigation of a pipe flow was conducted by Reynolds who discovered the law of similarity based on a dimensionless parameter which now is labeled by his name:

$$Re = \frac{ud}{\nu}, \tag{4}$$

where u is flow velocity, d is pipe diameter, and ν is kinematic viscosity of the fluid. In more general form applicable to any flow, u and d are considered as some "typical" flow velocity and flow scale that, in case of channel flow, called hydraulic diameter and defined as $d_h = 4A/\Pi$, where A is cross-section area of the channel and Π is wetted perimeter. Multiplier four is given to make d_h equal to the pipe diameter is the reference case of circular tube studied be Reynolds. The flows of different fluids in channels of different sizes (and, roughly, of different shapes) are similar when they defined by the same value of Reynolds number. One of the most fundamental facts is that there exists some *critical* Reynolds number Re_{cr} where flow becomes unstable and turbulent for all the higher Reynolds numbers. Reynolds himself found that Re_{cr} is between 11800 and 14300. So high values can be explained by using very smooth pipe inlet in Reynolds experiments. Latest numerous experiments discovered that $Re_{cr} \approx 2000$. Nevertheless, it is important to note here that in some other works, and first to mention in the experiment of Pfeninger [6], conducted on very smooth pipes, the laminar flow observed for Reynolds numbers up to 100000. The ratio length-to diameter was up to 600 and entire laminar flow was observed over all the length.

Suggesting that the experiments of Pfeninger [6] and others were correct, one should accept that laminar flow region cannot be limited by Reynolds number 2000. Then, we suggest that turbulent motions in wall-bounded channel flow are the result of finite-size perturbations causes either by wall roughness or inlet conditions. If the flow became unstable due to infinitively small disturbances that are always exist, the laminar flow would not be observed at any Reynolds number higher than critical. Furthermore, a precise value of this critical Reynolds number would be easy obtained by applying a linear instability analysis. If this conclusion is true, we suggest that there cannon be an "universal" theory of channel flow turbulence simply because real channels are different. However, for the most practical cases, turbulent flow in relatively smooth channels definitely behaves very similar developing the universal velocity profile. The wall influences the flow only for relatively large roughness at relatively high Reynolds numbers.

1.3 Flow Disturbances, Vortex Development and Statistics

The study of transition to the turbulence is occupied many researchers from the time of Reynolds until now making it very difficult referencing every paper in the field. In this work, we shell mention some works that provide a background for present investigation. Very detailed historical review following by discussion of careful experimental study was given by Wygnanski [7, 8].

When fluid enters a channel through the inlet that usually a smooth contraction from a large settling chamber, the cross-section velocity distribution changes with downstream distance. Initially, velocity profile is nearly uniform, but because of viscous effects, the profile changes downstream until flow reach a cross-section where a *fully-developed* velocity profile is attained. It means that from this cross-section downstream the flow becomes independent on the axial coordinate. If the Reynolds number is high enough, flow becomes instable and turbulent in some point. For relatively small Reynolds numbers slightly higher that critical value 2000, the rapid

transition of the flow from laminar to turbulent and then back to laminar can occur as shown in Fig. 1(a).

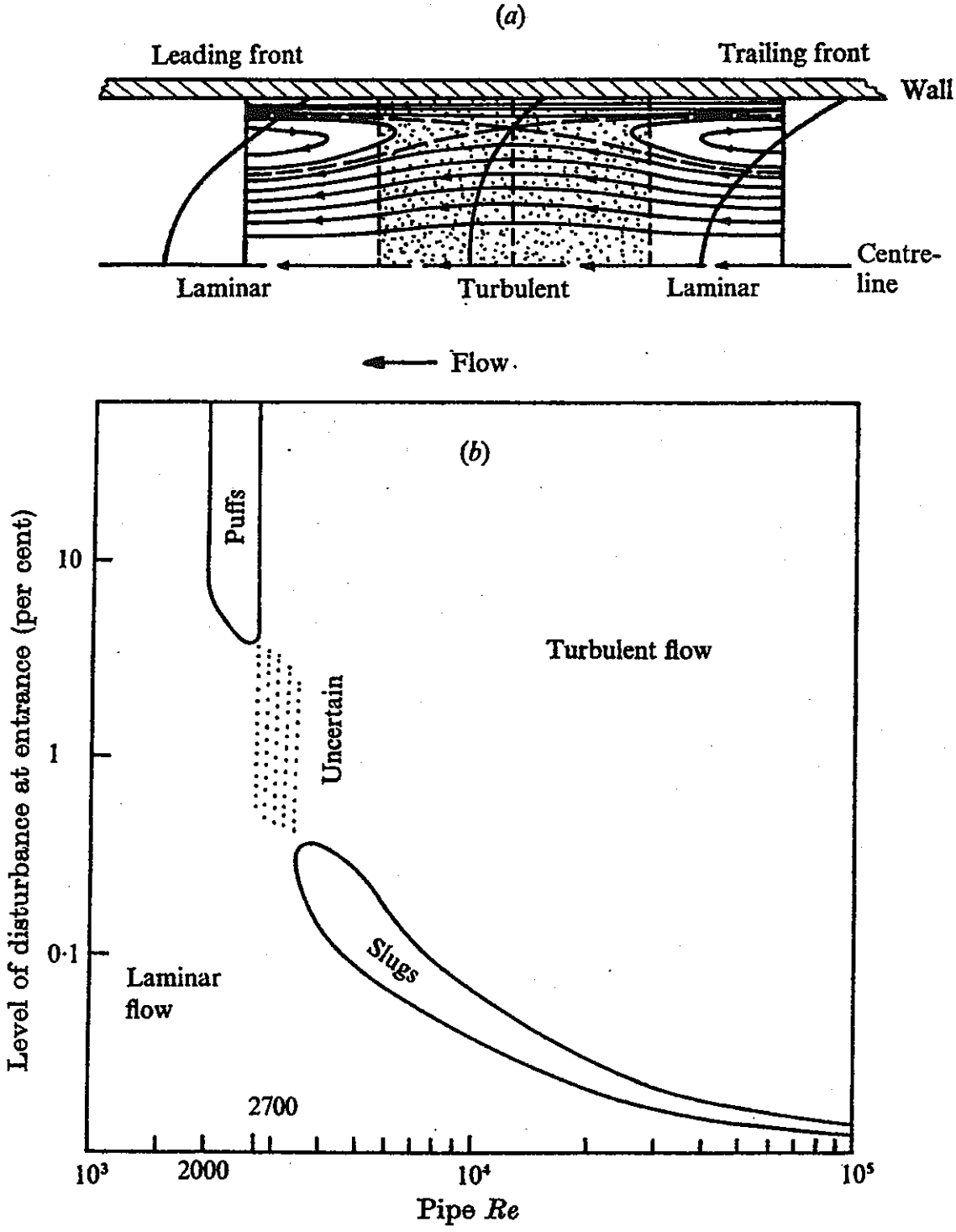

Figure 1. *(a) Schematic diagram of the flow in a turbulent slug*
(b) The regions in which slugs and puff occur in transitional pipe flow as a function of the disturbance level
by Experiment of Wygnanski [7]

Wygnanski [7] found experimentally two very different types of intermittently turbulent flow occurring naturally in a pipe:

- *Slugs*, which are caused by instability of of the boundary layer to small disturbances in the inlet region of the pipe and

- *Puffs*, which are generated by large disturbances at the inlet

While slugs are associated with transition from laminar to turbulent flow, puffs represent an incomplete re-laminarization process. Wygnanski [7] only observed puffs generation at $2000<Re<2700$, while slugs occurred at any $Re>3200$. In Fig. 1(b) the Reynolds numbers at which puffs and slugs occur are delineated as a function of the disturbance level at the entrance. This figure represents schematically the various regions encountered in transitional pipe flow at large distances from the inlet, i.e. at locations where the flow can be considered fully-developed. One can see that these data do not uniquely determine the critical Reynolds number at which transition occurs. In case of very low inlet disturbance flow can remain laminar even for Reynolds numbers up to 5000 (according to Wygnanski [7]).

Many other experiments, actual as well as virtual, numerical were performed to study the structure of turbulence, types of eddy developments, and nature or transition from laminar to turbulent flow. Among them, Eckelman [9] and Kreplin [10] studied the structure of the viscous Sublayer and behavior of fluctuating velocity in the wall region of turbulent channel flow. Thomas [11] reviewed up-to-date approaches for modeling of wall turbulence and proposed a model of transport mechanism associated with the turbulent burst phenomenon. A Dimensionless burst period was calculated and found to be independent on Reynolds number:

$$T^+ = \frac{u_\tau^2 \langle T \rangle}{\nu} \approx 14.93^2 \approx 223, \tag{5}$$

where $u_\tau = \sqrt{\tau_w / \rho}$ is dynamic, or friction, velocity; τ_w is wall shear stress, and $\langle T \rangle$ is mean burst period. This value correlates very well with experiment of Alp [12] who found that $T^+ \approx 250$ in a wide range of Reynolds numbers. It should be note here that dimensionless burst period corresponds to some "dynamic" Reynolds number defined as follows:

$$Re_\tau = \frac{u_\tau l_\tau}{\nu} = \frac{u_\tau^2}{\nu}\frac{l_\tau}{u_\tau} = \frac{u_\tau^2}{\nu}\langle T \rangle = T^+, \tag{6}$$

where average burst period is defined via dynamic velocity u_τ (that nearly the same as near-wall fluctuation velocity), and mean length of burst l_τ. Kirillov [13] used mean period of fluctuations in study of influence of wall conductivity to the turbulent heat exchange. In recent private communications, P.L. Kirillov mentioned similarity above (Eq. (6)) between dimensionless T^+ and Re_τ. This is in support of the central idea of MSV assuming an existence of the *universal* Reynolds number.

Numerical simulation in a plane channel with a sudden expansion was performed by Mizushima [14]. Experimental observations show that flow in symmetric channel makes a transition from symmetric flow to asymmetric one due to a symmetry-breaking pitchfork bifurcation on a gradual increase of the Reynolds number. Numerical simulation could not confirm this for perfectly symmetric systems. However, when slightly asymmetric boundary conditions were given, calculation demonstrated asymmetric bifurcation similar to experimental observations. Though the present work is limited by fully-developed turbulent channel flows, we see one more flow sample that remains stable to infinitesimal disturbance for all Reynolds numbers range but can easily go unstable because of finite-size "imperfectness" in symmetry.

Bradshaw [15] discussed the influence of wall roughness on turbulent flow at high-Reynolds numbers. The concept of the "critical roughness height" is under the doubt. Analysis shows that Nikuradse [16] performed the experiments on close-packed sand roughness of uniform size. Considering new detailed measurements on "natural" pipes found in engineering, Bradshaw

concluded that "the effects of small roughness vary as power of roughness Reynolds number... then one can say only that the errors would become smaller, and eventually negligible, as Roughness Reynolds number decreased". We add, that if the latter is true, one should conclude that there are no really *smooth* pipes but *relatively* smooth walls to neglect roughness effects. In addition, should we suggest that in such an ideal pipe existed along with ideal inlet conditions, flow would be always laminar and would not depend on the pipe Reynolds number? Another uncertainty is whether the flow in a long ideal pipe changes to laminar at infinity.

The shape and frequency (both in space and in time) of imperfect disturbances are also very important and were recently studied intensively with advance of measurement technique. Eliahou, Tumin, Han and Wygnanski [17, 18] studied experimentally the influence of artificial periodic perturbations emanating from the wall on the transition to the turbulence. Vincont [19] measured viscosity and scalar concentration fields in the plume emitting from a two-dimensional line source at the wall. Andersson [20] performed direct numerical simulation of developing natural disturbances in a flat boundary layer.

As for the developed turbulent flow, the vortex organization and development can be found in experiments of Adrian [21] where the structure of energy-containing turbulence in the outer region of zero-pressure-gradient boundary layer has been studied. Though these data are related to the boundary layer flow, they can be used as reference in channel flow modeling due to a lack of detailed measurements in pipe and plane channel flows.

Detailed data on fully-developed turbulence structure including timescale velocity distributions and statistical moments are vital for turbulence modeling both as a source of empirical knowledge and reference for numerical predictions. Johansson [22] measured streamwise velocity component on fully-developed water-channel flow for three different Reynolds numbers (13800, 34600 and 48900).

Kim [23] performed a direct numerical simulation of turbulent flow in a plane channel. The Navier-Stokes equations were solved in three dimensions at low Reynolds number of 3300, with about four millions grid nodes. All "essential" turbulence scales were resolved and no subgrid model was used. Numerical results were compared with experimental measurements at low Reynolds numbers. Kim found that although the general characteristics of the computed turbulence statistics were in a good agreement with experimental results, detailed comparison in the wall region revealed consistent discrepancies. In particular, the predicted Reynolds stresses, both normal and shear stresses were consistently lower than the measured values. Kim pointed that same disagreement could be found in other numerical works and suggested the possible reason would be inaccurate near-wall measurements. In another numerical simulation, Spalart [24] studied the turbulent boundary layer on a flat plate with zero pressure gradient. Again, time-dependent Navier-Stokes equations were solved in three dimensions by spectral method using about ten millions grid points. Results showed a good agreement with experimental data in general. The most significant discrepancy (about 5%) was the friction factor at the highest Reynolds number that was $Re_\theta=1410$ (based on the boundary layer thickness).

1.4 Experimental Data for Velocity Profile, Eddy Diffusivity and Friction Factor

Detailed experimental measurements of velocity profile and statistics are very important for the turbulence modeling due to the following main reasons:

- Experiments provide the necessary empirical base for models of turbulence
- The validity of modeling should be verified by comparison with experiment

Although both statements above may seem identical, the difference is that former provide an input for the model while later is related to the output. And those experimental data are not necessary the same. For example, results of modeling are easy to compare with experimental

velocity profile and friction factor. However, calculating turbulent viscosity via experimental velocity profile may be not accurate because of uncertainty and measurement errors. Certainly, turbulent viscosity can be easily found by differentiating velocity profile. Let us consider a fully-developed turbulent flow in a circular tube. Reynolds equations are reduced to single one-dimensional equation like following:

$$\frac{1}{\rho}\frac{d\langle p\rangle}{dz}=\frac{1}{r}\frac{\partial}{\partial r}\left(r\left(\nu+\nu_{turb}\right)\frac{\partial\langle u\rangle}{\partial r}\right), \tag{7}$$

where $\langle p\rangle$ is pressure, r and z are radial and axial coordinate correspondently. Since the pressure gradient is constant, turbulence viscosity can be easy obtained from Eq. (7):

$$\nu_{turb}=\frac{\frac{r}{\rho}\frac{d\langle p\rangle}{dz}}{2\frac{\partial\langle u\rangle}{\partial r}}-\nu=\nu\left(\frac{r\left.\frac{\partial\langle u\rangle}{\partial r}\right|_{w}}{r_{w}\frac{\partial\langle u\rangle}{\partial r}}-1\right), \tag{8}$$

where subscript index w is assigned to the wall values. Since the gradient of axial velocity is used as denominator, even small error in velocity profile results in much higher error in turbulent viscosity distribution. If velocity profile is given by the set of N velocity values, one can calculate numerically turbulent viscosity distribution as follows:

$$\nu_{turb}^{i}=\nu_{turb}\left(\frac{r_{i+1}+r_{i}}{2}\right)=\nu_{turb}\left(r_{i+1/2}\right)=\nu\left(\frac{r_{i+1/2}\left.\frac{\partial u}{\partial r}\right|_{w}}{r_{w}\frac{u_{i+1}-u_{i}}{r_{i+1}-r_{i}}}-1\right). \tag{9}$$

Using Eq. (9), let us calculate turbulent viscosity distribution based on the experiments of Zagarola [25, 26] conducted on Princeton's "SuperPipe" facility. SuperPipe was constructed to investigate a fully developed turbulent pipe flow over a large range of Reynolds numbers. SuperPipe experiments were performed in a very large range of Reynolds numbers, 3.1E+4 to 3.5E+7 that provide an excellent reference base for pipe flow calculations. Axial velocity was measured at 52 locations starting from 0.45mm from the wall. However, as it was mentioned above, even precise and detailed data on velocity profile cannot guarantee accuracy in turbulent viscosity distributions. Figure 2(a) shows velocity profiles from SuperPipe experiment [25] for two Reynolds numbers, low and high. For the reference, velocity profiles calculated with experimental formula of Reichardt [27] are given by solid lines. Reichardt's formula was applied to the same locations of points given by SuperPipe experiment but symmetrically extended to the opposite wall. Both profile are in a very good agreement. Distributions of turbulent viscosity calculated from SuperPipe and Reichardt's velocity profiles are shown in Fig. 2(b). The same profiles versus logarithmic dimensionless coordinate $y^{+}=yu_{\tau}/\nu$ are shown in Fig. 3. One can see that those results cannot satisfy even minimal accuracy requirements.

a)

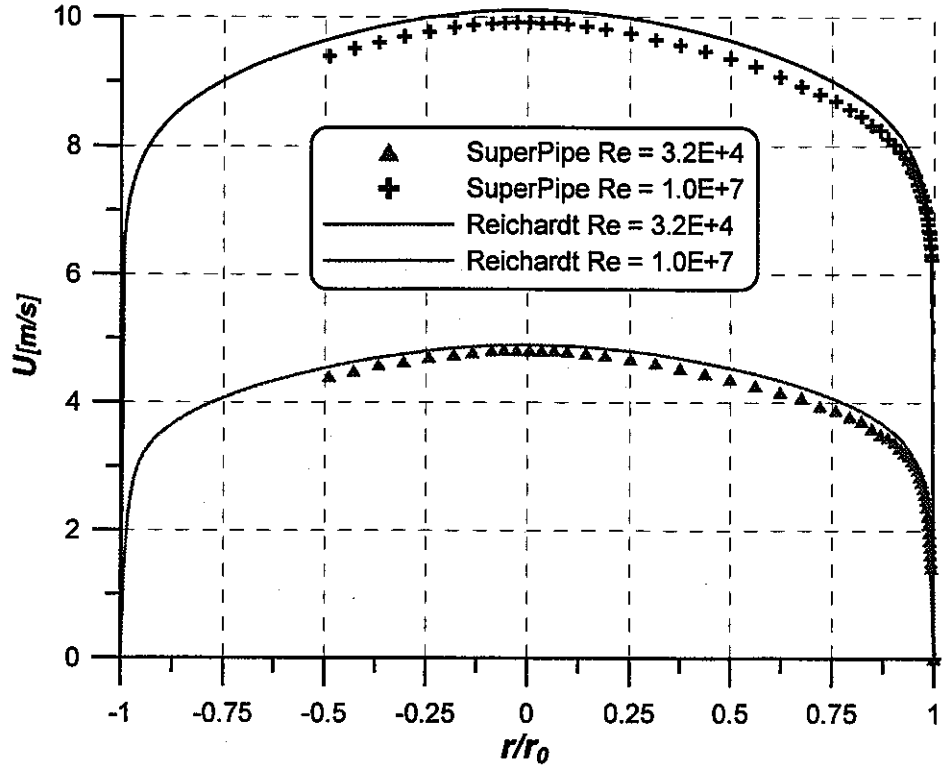

b)

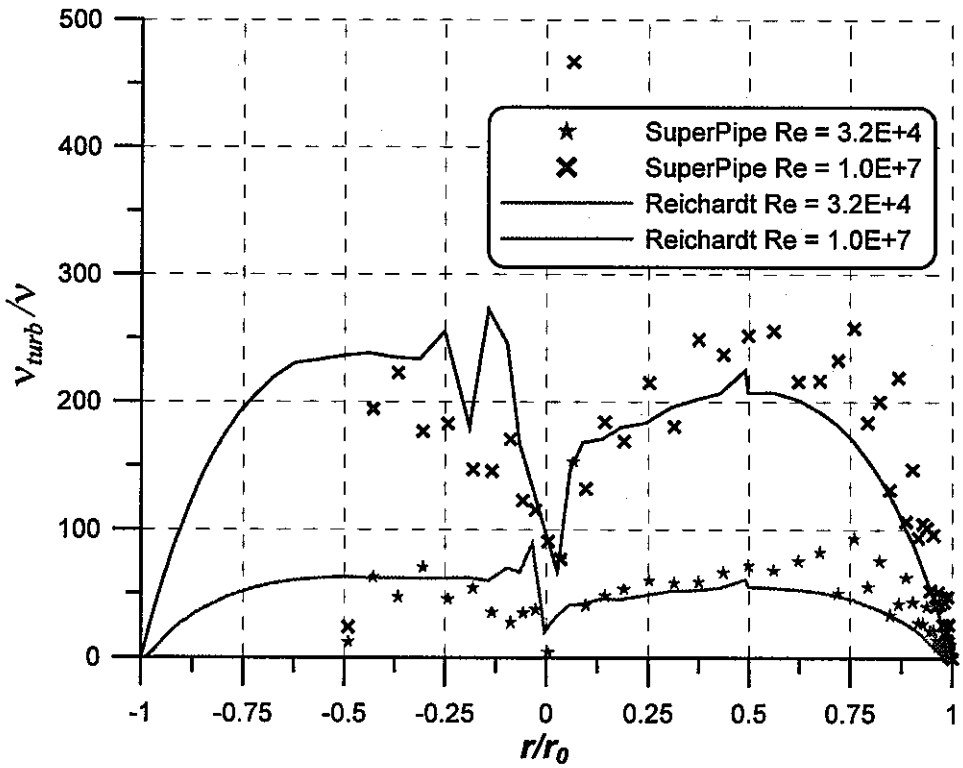

Figure 2. Calculation of turbulent viscosity(b) from SuperPipe experimental velocity profiles(a) of Zagarola [25]
Solid lines refer for the same calculations based on the Reichardt's profile formula

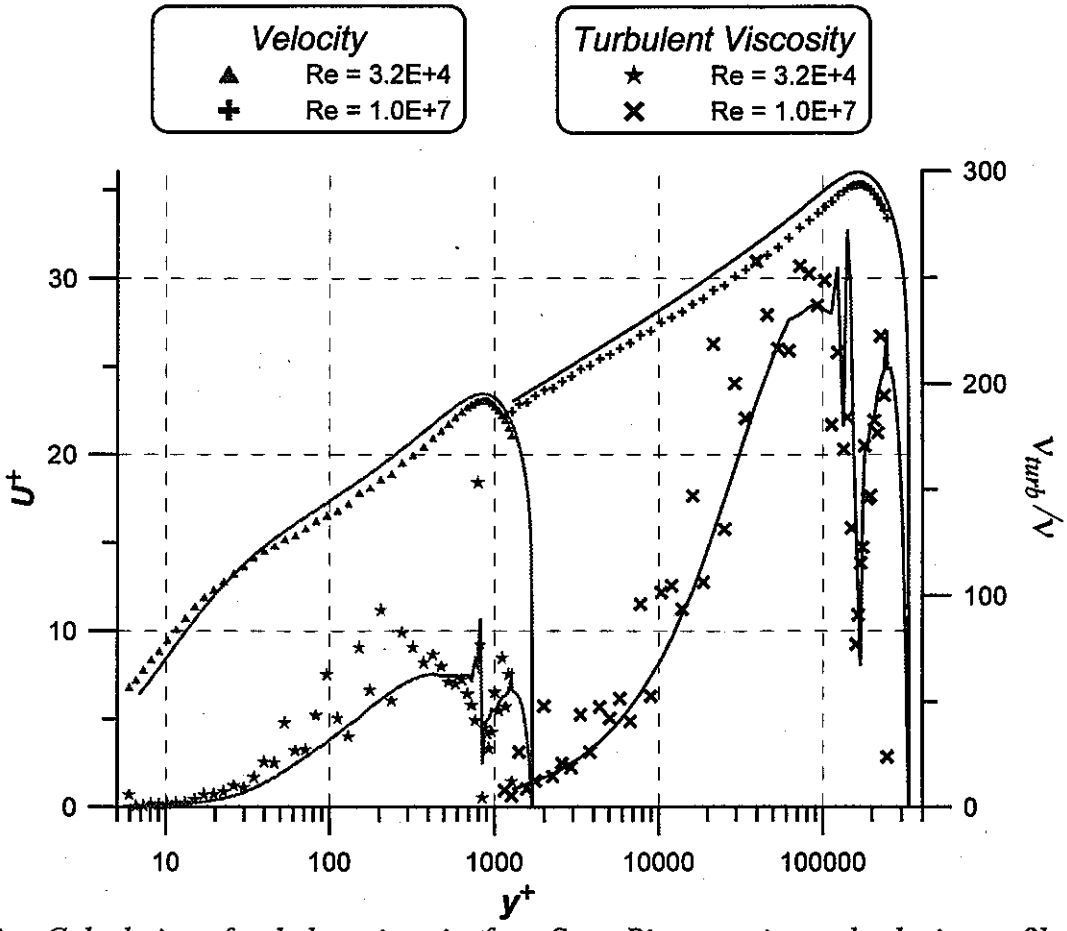

Figure 3. Calculation of turbulent viscosity from SuperPipe experimental velocity profiles of Zagarola [25] vs. dimensionless distance to the wall
Solid lines refer for the same calculations based on the Reichardt's profile formula

As for the Reichardt's formula, its results can be easy smoothed by increasing the number of points in the data set. However, for experimental data, only three options are available:

- to apply some smoothing algorithm for velocity profile
- to increase significantly the number of measurement locations
- to measure second-order moments including Reynolds shear stresses directly

Probably only the later can guarantee a good accuracy. Unfortunately, this kind of detailed transient measurements is very difficult for channel flows. However, such data can be found in many available experiments for the boundary layer flows. The good review and assessment of boundary layer experimental data was performed by Sreenivasan [28] and, later, by Fernholz [29]. Recently, very detailed measurements of Reynolds stresses for a flat-plate boundary layer in a wide range of Reynolds numbers were performed by DeGraff [30]. In the present work, doing with the MSV model, we will concentrate on the fully-developed channel flow. Nevertheless, detailed experimental data for the boundary layer flow help to understand the structure and features of turbulent flow in general as well as give a way for the extension of MSV for the other types of turbulent flows. Figure 4 shows velocity profiles measured in DeGraff [30] experiment. Here, the Reynolds number is defined by boundary layer thickness and velocity: $Re_\theta = u_\theta \theta / \nu$.

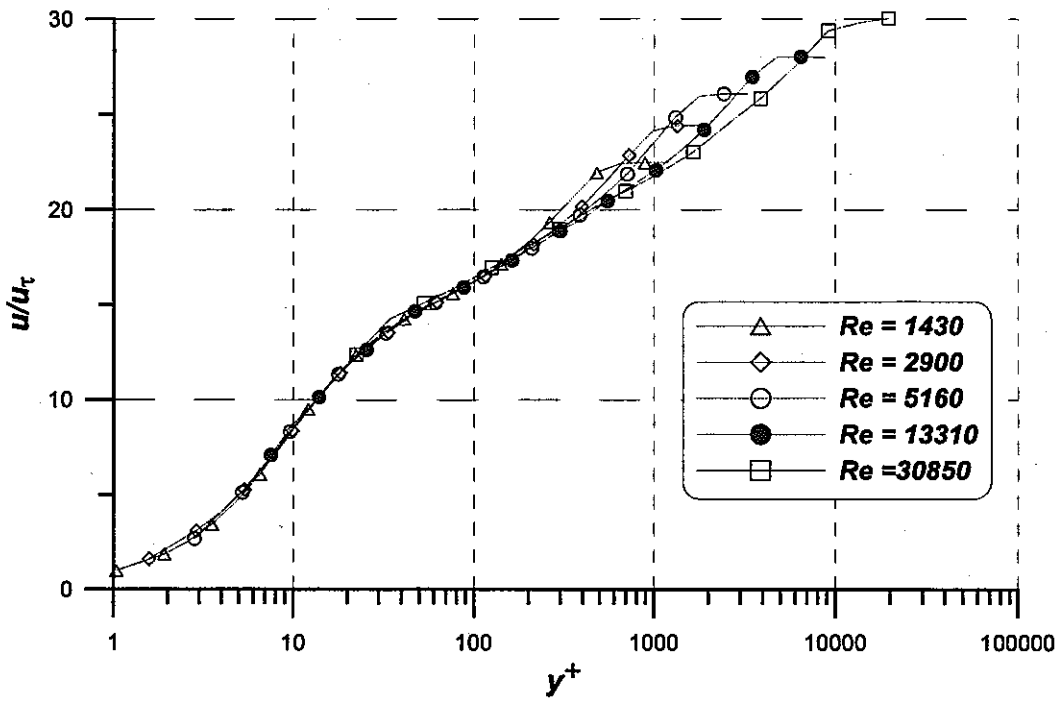

Figure 4. Dimensionless velocity profiles by experiment of DeGraff [30]
Reynolds number is based on the thickness θ and the outer speed of the boundary layer
u_θ: $Re_\theta = \frac{u_\theta \theta}{\nu}$

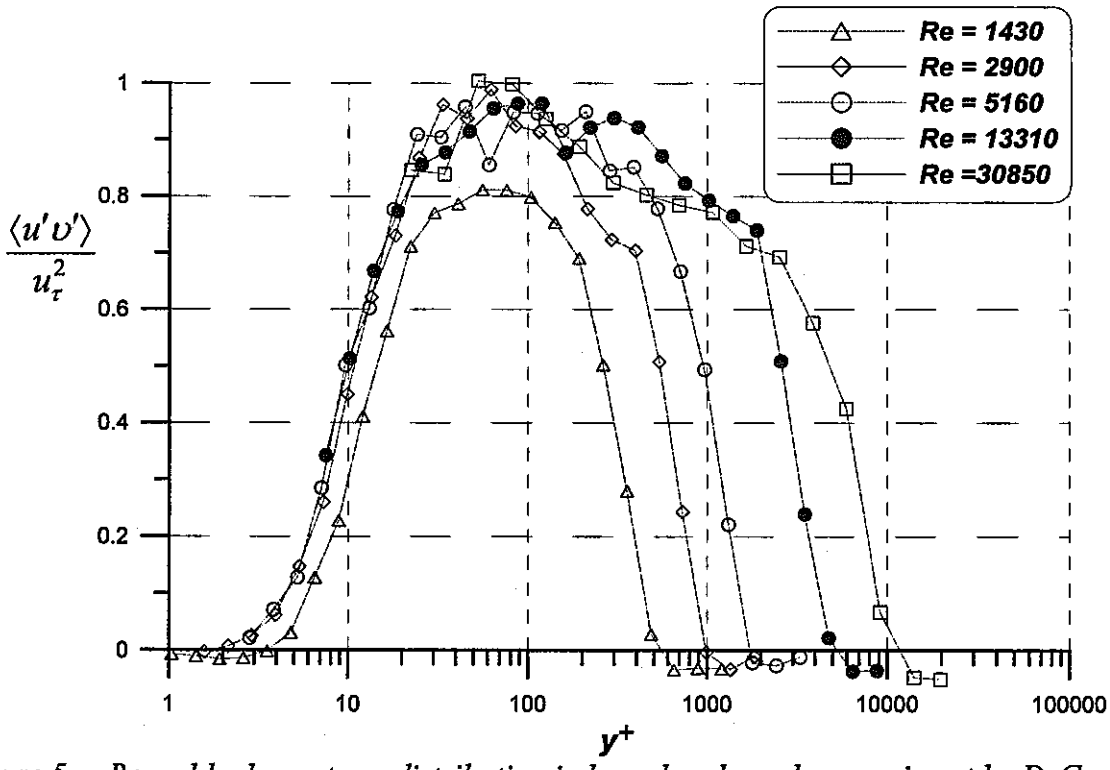

Figure 5. Reynolds shear stress distribution in boundary layer by experiment by DeGraff [30]
$Re_\theta = \frac{u_\theta \theta}{\nu}$

Second- and even third-order moments were measured directly in DeGraff [30] experiment. The distribution of Reynolds shear stresses is shown in Fig. 5. One can see that velocity profiles are

very smooth (Fig. 4) but the accuracy of shear stress measurements is not very good. There are some unphysical oscillations in the outer region of boundary layer. Also, some values for shear stress become even negative near the wall and in the core flow region. Nevertheless, accuracy of the DeGraff's measurements is good enough to compare with result of turbulence modeling.

1.5 Experimental Velocity Scaling Laws and Theoretical Models

The other good source of model verification is the velocity scaling laws which based mainly on the analysis of many other experimental data. Barenblatt [31, 32, 33] proposed a non-universal (i.e. depending on the Reynolds number) for the mean velocity distribution in fully-developed turbulent shear flows including channel flows and wider classes, such as boundary layers. The proposed scaling law involves a special dependence of the power exponent and multiplication factor on the flow Reynolds number. It emerges that universal logarithmic law is closely related to the envelope of a family of power-type curves each corresponding to a fixed Reynolds number. Barenblatt [32] compared the model with available experimental data (mainly from Nikuradse [16]) and found a good agreement both for velocity profiles and skin-friction factor.

Wosnik [34] proposed a theory for fully-developed pipe and channel flows. This theory also extends classical universal velocity profile approach to include the effect of finite Reynolds numbers. In the limit of infinitive Reynolds number, these reduce to the familiar law of the wall and velocity deficit law respectively. Wosnik [34] introduced a *mesolayer* near the bottom of the overlap region approximately bounded by $30 < y^+ < 300$ where there is not the necessary scale separation between the energy and dissipation ranges for inertially dominated turbulence. The experimental data from the SuperPipe experiment of Zagarola [26] at Princeton and direct numerical simulation (DNS) of plane channel flow by Kim [23] were carefully examined and shown to be in excellent agreement with Wosnik's theory over the very large range of Reynolds numbers.

The MSV model does not predict the universal velocity profile, independent on the Reynolds number. Thus, it is important to compare MSV results not only with experimental data but also with some physical models described in this section.

2. FORMULATION OF MULTI-SCALE VELOCITY MODEL OF TURBULENCE

2.1 Energy-Balanced Turbulent Reynolds Number

First of all, let us suggest possible physical explanations for the Reynolds number $Re = ul/\nu$. Generally, the Reynolds number indicates the intensity of turbulence: the higher Reynolds number – the higher flow turbulence. And vice versa, for low Reynolds numbers, the turbulence does not occur or, at least, is very unlikely.

Schlichting [35] suggested that physically, Reynolds number is a ratio of *inertia* forces to *friction* forces. This theory is supported by good reasoning for external boundary layers around solid obstacles where flow changes its direction. However, there are no inertia forces neither in straight channel flows nor in plane boundary layers. Another possible treatment of Reynolds number is as ratio of turbulent energy production ($\rho u^3/l$) to the corresponding energy dissipation ($\mu u^2/l^2$) (from private communication with P.L. Kirillov).

From analysis of dimensions, few physical explanations of Reynolds number are possible. Let us suggest that Reynolds number represent a balance of energies. For example, it is ratio of flow kinetic energy to the work of friction forces inside the same volume of fluid:

$$Re_e = \frac{Kinetic\ Energy}{Work\ of\ Friction} = \frac{K}{W}. \tag{10}$$

Work of friction forces W can be calculated as follows:

$$W = \iiint_V \tau_{ij} dV = \iiint_V \mu \frac{\partial u_n}{\partial n} \vec{n} dV. \tag{11}$$

For the laminar flow in a circular tube, formula (11) can be rewritten as:

$$W = 2\pi z \int_0^{r_0} \mu \left| \frac{\partial u}{\partial r} \right| r dr = \frac{8}{3} \pi r_0 z \mu \bar{u}, \tag{12}$$

assuming that velocity profile is given by:

$$u(r) = 2\bar{u}\left(1 - \frac{r^2}{r_0^2}\right), \tag{13}$$

where r_0 is pipe radius, z is axial coordinate, and $\bar{u}$ is mean velocity, averaged over the area of integrating (i.e. whole the pipe in this case).

Kinetic energy of entire flow can be written as:

$$K = \iiint_V \frac{\rho u^2}{2} dV = \frac{\rho \langle u^2 \rangle V}{2}. \tag{14}$$

Again, for the pipe flow it reduces to

$$K = 2\pi z\rho \int_0^{r_0} \frac{1}{2} u^2 r dr = \frac{4}{3}\pi r_0^2 \rho z \bar{u}^2 . \tag{15}$$

Then, dividing (15) by (12), one can obtain *energy-based* Reynolds number as follow:

$$Re_e = \frac{K}{W} = \frac{1}{2}\frac{r_0}{\mu}\rho\bar{u} = \frac{Re}{4}. \tag{16}$$

Formula (16) is obtained for the laminar pipe flow. What is happening if we apply the same procedure to the turbulent flow? Let us do integrating above for the turbulent velocity profile obtained by Reichardt [27]:

$$u^+ = \frac{u}{u_\tau} = 2.5\ln\left(\frac{1.5\left(1+0.4y^+\right)\left(1+\frac{r}{r_0}\right)}{1+2\frac{r^2}{r_0^2}}\right) + 7.8\left(1-\exp\left(-\frac{y^+}{11}\right)-\frac{y^+}{11}\exp\left(-0.23y^+\right)\right). \tag{17}$$

Formula (17) describes experimental data for pipes very well but analytical integration and differentiation is difficult. For simplicity, we use numerical integration with very fine mesh (10000 grid points on irregular mesh system with fine near-wall resolution). All calculations were also performed on a mesh with 1000 grid points and no visible discrepancy was found. Using Reichardt's formula (17), the following energetic Reynolds number was calculated:

$$Re_e = \frac{K}{W} = \frac{2\pi z\rho \int_0^{r_0} \frac{1}{2} u^2 r dr}{2\pi z \int_0^{r_0} \mu \left|\frac{\partial u}{\partial r}\right| r dr} = \frac{1}{2}\frac{\rho\langle u^2\rangle}{\mu\left\langle\left|\frac{\partial u}{\partial r}\right|\right\rangle}. \tag{18}$$

Figure 6 shows dependence of the energy-based Reynolds number on regular one. Surprisingly, relation (16) is valid not only for laminar flow but for turbulent region as well, even for the high Reynolds numbers. It should be mentioned however, that denominator in Eq. (18) actually does not represent the work of friction forces for the turbulent flow. Real friction is contributed by Reynolds stresses (dissipation of turbulence) and should be much higher that simple product of molecular viscosity and mean axial flow gradient. Nevertheless, energy Reynolds number given by Eq. (18), that is actually the same as regular, helps to give a physical meaning to the Reynolds number as a *ratio of total kinetic energy of the flow to the work of friction that should occur in a laminar flow with the same velocity profile.*

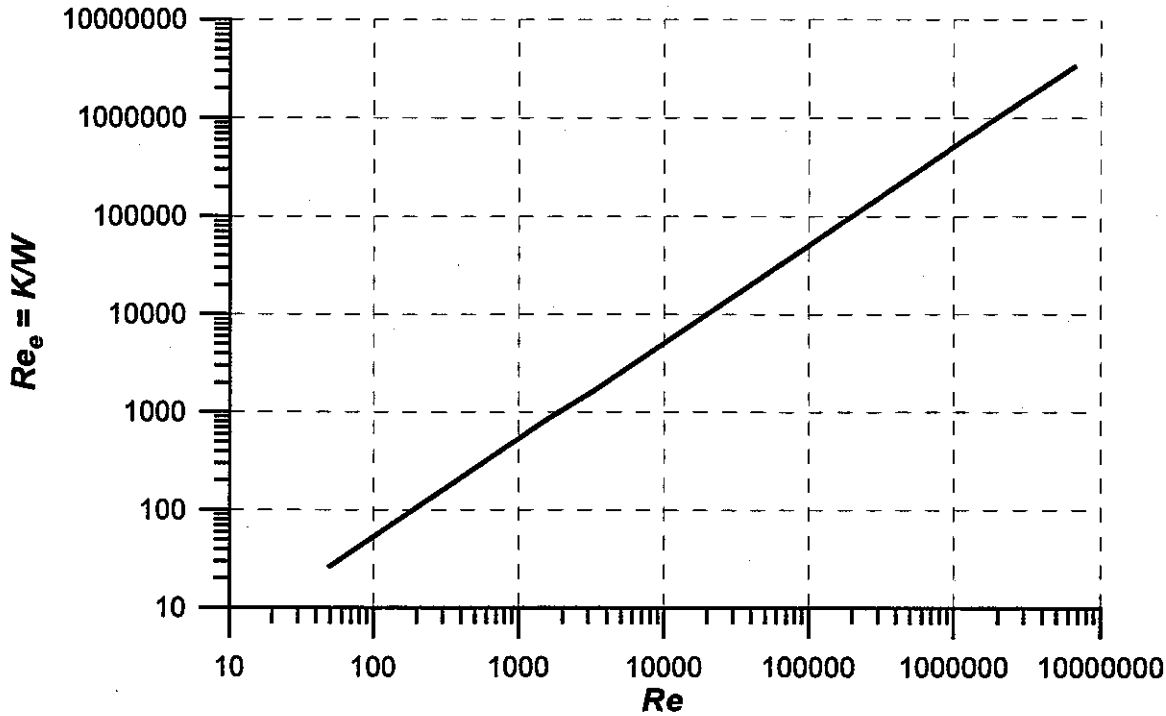

Figure 6. Energy-based Reynolds number versus regular Reynolds number

Let us consider now another possibility of Reynolds number definition. In a turbulent flow, two controversial trends can be considered:

- *Velocity profile intends to be flat.* As we mentioned many times before, there always exist turbulent vortexes that transport energy from lower speed region to higher speed energy and vice versa. Energy losses (dissipation) occur because of mixing high and low speed eddies. The flatter velocity profile is – the lower energy spends on dissipation.
- From the other hand, *average velocity gradient intends to be small* to lower skin friction energy loss.

These contradictory factors shape resulting velocity profile for the turbulent flow. In case of the laminar flow, there is no vortexes and no energy transport. Therefore, the laminar flow profile is shaped by minimal average velocity gradient only.

Taking in mind trends above, let us suggest a universal criterion for the turbulent flow conditions. We shell use the same idea about kinetic energy to friction work ratio. Let us define a kinetic energy of profile *flatorization*, or an energy that is released when flow is completely mixed, or become flat:

$$K = \iiint_V \frac{\rho u^2}{2} dV - \frac{\rho \bar{u}^2}{2} V = \frac{\rho V}{2}\left(\langle u^2 \rangle - \bar{u}^2\right). \tag{19}$$

The work of friction is defined as a total energy loss because of friction including Reynolds shear stress:

$$W = \iiint_V \tau_{ij} dV = \iiint_V \left(\mu \frac{\partial u_n}{\partial n} \vec{n} - \langle u_i' u_j' \rangle \right) dV . \tag{20}$$

Let us apply integrals (19) and (20) to the pipe flow as shown in Fig. 7.

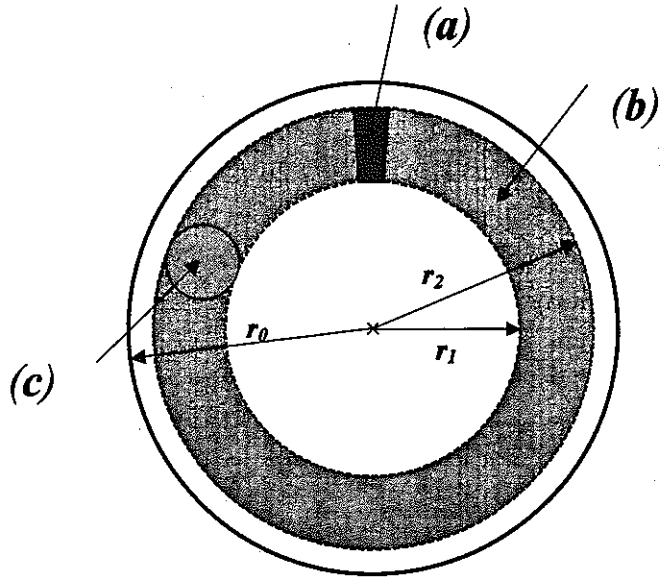

Figure 7. Pipe flow: Areas of Integration

If the area between radius r_1 and r_0 is considered, two types of integration area shown in Fig. 7 are possible:

a) Non-weighted integration:

$$K_V = \frac{1}{2(r_2 - r_1)} \int_{r_1}^{r_2} u^2 dr - \frac{1}{2(r_2 - r_1)^2} \left(\int_{r_1}^{r_2} u dr \right)^2, \tag{21}$$

$$W_V = \frac{1}{(r_2 - r_1)} \int_{r_1}^{r_2} \left(\mu \frac{\partial \langle u \rangle}{\partial r} - \langle u' \upsilon' \rangle \right) dr = \frac{1}{(r_2 - r_1)} \int_{r_1}^{r_2} (\mu + \rho v_t) \frac{\partial \langle u \rangle}{\partial r} dr \tag{22}$$

b) Annular area weighted integration

$$K_V = \frac{1}{\left(r_2^2 - r_1^2\right)} \int_{r_1}^{r_2} u^2 r dr - \frac{2}{\left(r_2^2 - r_1^2\right)^2} \left(\int_{r_1}^{r_2} u r dr \right)^2, \tag{23}$$

$$W_V = \frac{2}{\left(r_2^2 - r_1^2\right)} \int_{r_1}^{r_2} \left(\mu \frac{\partial \langle u \rangle}{\partial r} - \langle u' \upsilon' \rangle \right) r dr = \frac{2}{\left(r_2^2 - r_1^2\right)} \int_{r_1}^{r_2} (\mu + \rho v_t) \frac{\partial \langle u \rangle}{\partial r} r dr. \tag{24}$$

Figure 8 shows numerically calculated $Re_t = \frac{K}{W}$, which we call a *turbulent* Reynolds number defined for three flow areas.

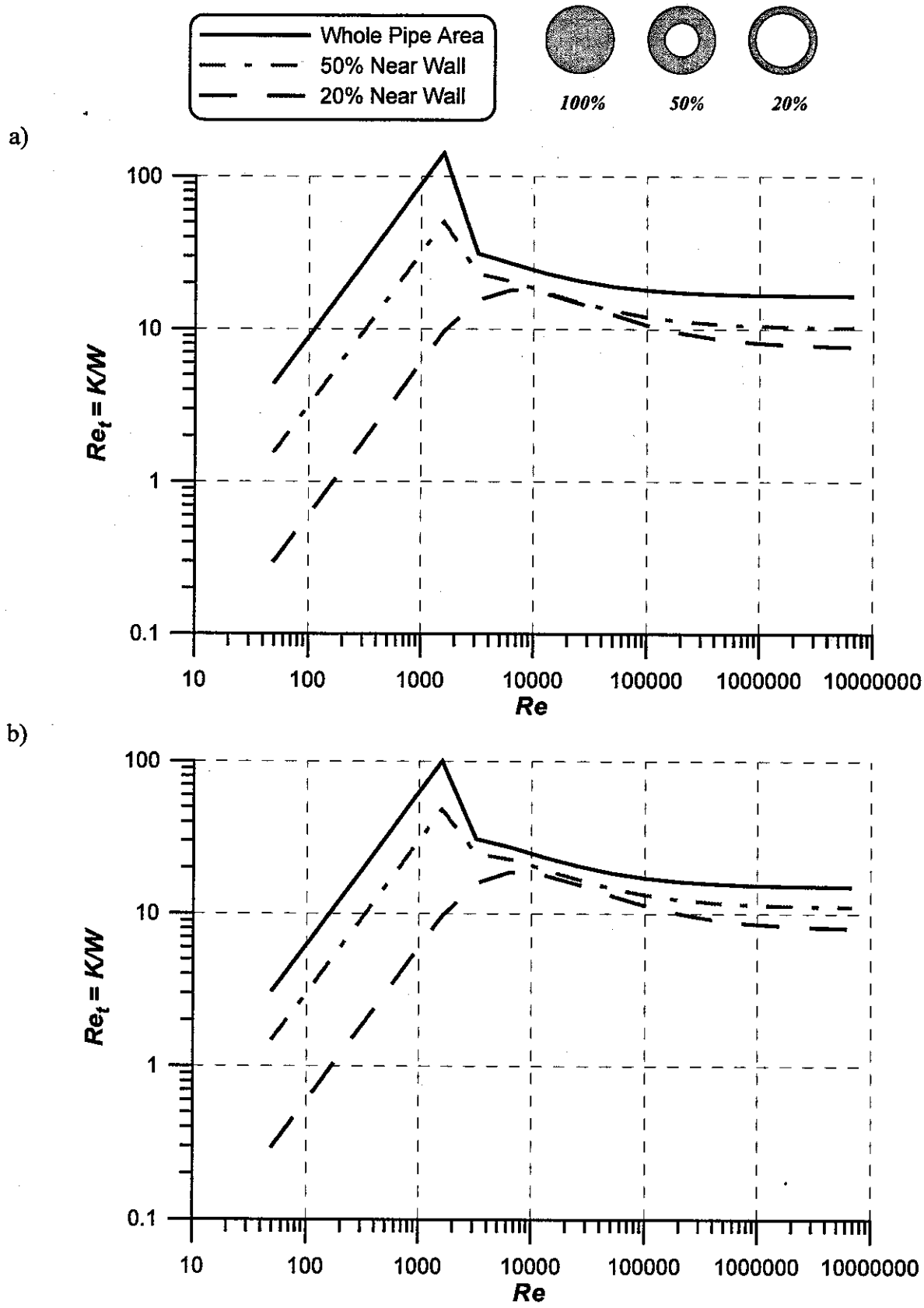

Figure 8. Turbulent Reynolds number versus regular Reynolds number
a) no-radius weighted integration over (a) area on Fig.
b) radius-weighted integration over (b) area

One can see that Re_t grows linearly within laminar region, reaches its maximum near the critical point Re=2000, and then directs to some constant value that ranges from about 8 to 11 depending on integration area. We suggest that for every fluid area:

There exists a turbulent Reynolds number Re_t that never exceeds some critical, constant and universal value.

Re_t is defined as balance of kinetic energy given by Eq. (19) and work of friction forces Eq. (20). Knowing the value of this turbulent Reynolds number, one can calculate the turbulence viscosity distribution for a given velocity profile, and, at the end, calculate the final velocity and turbulent distributions that satisfy non-exceeding Re_t condition at every point of the fully-developed channel flow. It will be elaborated in the following section. Here, we would like to mention that the critical turbulent Reynolds number is the only experimental value in the MSV model. It also can be estimated from the following experimental fact. For the all turbulent flows, there exist a laminar sublayer near the wall where $u^+=y^+$ that is limited by $y^+<5$. Then, by integrating the laminar velocity profile, one can easy find that near the wall within laminar sublayer:

$$Re_t = \rho \frac{\langle u^2 \rangle - \langle u \rangle^2}{\mu \left\langle \frac{\partial u}{\partial y} \right\rangle} = \frac{\frac{u_\tau^2}{3} y_0^{+2} - \frac{u_\tau^2}{4} y_0^{+2}}{u_\tau^2} = \frac{y_0^{+2}}{12} \approx 8.33, \tag{25}$$

Here, we assumed that no turbulence occur at $y^+=5$ point so the total integration area in Eq. (25) is $y_0^+ = 10$.

It should be noted that, for the moment, we consider only fully-developed wall-bounded flows. However, we also believe the same hypothesis can be extended to zero-gradient boundary layers and, perhaps, to wide types of the turbulent flows.

The behavior of the plots in Fig. 8 generally supports the turbulent Reynolds number hypothesis. However, several question arise that can doubt this. In ideal, unlike plots shown in Fig. 8, the turbulent Reynolds number should grows in laminar area and stays at the constant level (below critical Re_t) after reaching turbulent regimen. Let us formulate the problems and suggest a possible explanation.

1. Why the turbulent Reynolds number exceeds significantly the critical value within and around the transition region? As one can suggest from Fig. 8, transition to the turbulence should start at $Re \approx 200$, where the whole pipe flow reaches critical value $Re_t \approx 10$, but not near the classical $Re \approx 2000$. However, the "classical" transient is observed in relatively smooth channels with relatively quiet inlet condition. Since the turbulent Reynolds number is a balance of kinetic energy change and friction forces sourced in possible energy dissipation by vortexes, it is suggested that these vortexes or other kinds of perturbations of scales comparable with the scale of the channel. Then, it may be suggested that near-turbulent, or similar-to-turbulent motions, can exist and expand in presence of large-scale perturbation as shown schematically in Fig. 9. Of course, this should be confirmed experimentally. All the experiments and numerical simulation of transition we reviewed, deal with higher Reynolds numbers and smaller perturbations.
2. The turbulent Reynolds number reaches the critical value smoothly, after approximately Re>10E+5, not after transition region, as one could expect.

3. The discrepancy between different integration areas is big enough as in the value ($8 \leq Re_t \leq 10$), as well as in the slope. That is natural for laminar flow but in disagreement with critical turbulent Reynolds number theory.

The answer to the later questions 2 and 3 is not easy. Nevertheless, we may suggest that:

- The Reichardt formula (17) used in these calculation is not necessary correct. Even smooth and well-fitted experimental velocity profiles do not guarantee the same smoothness in turbulent viscosity and Reynolds shear stress distributions derived by differentiating of the measured data or experimentally obtained formulas as was shown in introduction (see Fig. 2,5).
- The integration area is not necessary (a) or (b) type as shown in Fig. 7. It may be different, for example (c)-type shown in the same figure. For the moment, it is still unclear for us which type of integration to use. Definitely, it should reflect the way in which vortexes are developed in the flow. In other words, the energy balance should be applied to area where eddies can move, exchange the momentum and dissipate the energy.
- The last, but not least, is that an actual work of friction forces must include Reynolds shear stresses from the other two directions $\langle u'w' \rangle$ and $\langle \upsilon'w' \rangle$ of stress tensor to satisfy the full energy balance. For the moment, it is not clear how to model these moments. We hope to elaborate it in a future.

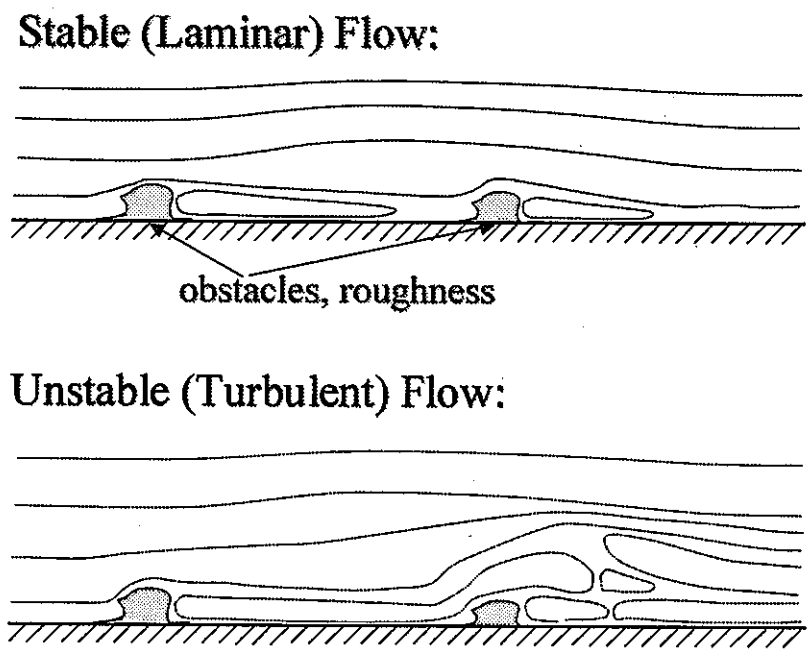

Figure 9. Laminar and near- turbulent flow at low Reynolds numbers

In spite of the problems above, we believe that an original idea of the turbulent Reynolds number and its critical value is entitled to be studied and verified. In the following section, we discuss the Multi-Scale Viscosity (MSV) model of turbulence that is based on these principles.

2.2 Calculation of Turbulent Viscosity Based on Critical Turbulent Reynolds Number

Following the idea of previous section, we assume that deformation of axial velocity within the area with scale l generates an extra turbulence for the given scale that keeps the local turbulent Reynolds number, defined for this scale, below some critical value. Here, the main question is the appropriate definition of the turbulent Reynolds number. As it was mentioned, very preliminary results are reported in this work. Additional researches are necessary to improve the model and find the proper physical criteria for the turbulent Reynolds number.

Let us start with very simple definition of the local Reynolds number. Let us define it as

$$Re_t = \frac{\Delta U\, l}{\nu + \nu_t^l}, \tag{26}$$

where ΔU is a velocity deformation for the scale l, and ν_t^l is an additional compensative turbulent viscosity for the given area. In the schematic view of the channel flow shown in Fig. 10, ΔU is defined as simple difference between axial velocities taken at the ends of the corresponding scale l. Then, if the turbulent Reynolds number calculated by Eq. (26) is higher then some experimentally found critical value Re_{cr}, the value turbulent viscosity at the middle point of scale is calculated as follows:

$$\nu_t^l = \frac{\Delta U\, l}{Re_t} - \nu, \tag{27}$$

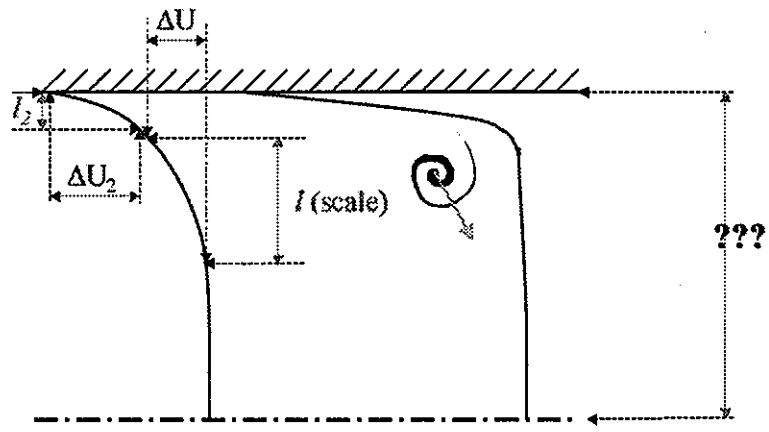

Local Reynolds number: $Re \sim \dfrac{\Delta U\, l}{\nu_{mol} + \nu_{turb}}$

Figure 10. Velocity profile in a channel

Again, if we assume that, there exist a laminar sublayer near the wall where $u^+ = y^+$ that is limited by $y^+ < 5$. Then, by integrating the laminar velocity profile, one can easy find that within laminar sublayer:

$$Re_t = \frac{u(2y_0)\,2y_0}{\nu} = \frac{u^+(2y_0^+)u_\tau\ \nu\dfrac{2y_0^+}{u_\tau}}{\nu} = 4y_0^{+2} \approx 100. \tag{28}$$

In actual calculations, we accepted the value of critical turbulent Reynolds number as Re_{cr}=130 because it fits better the friction factor calculations.

In the following, we shell refer to the MSV model that uses Reynolds number defined by Eq. (26), as *first-type* MSV, or simply MSV-1. The second type of the MSV model that is based on the energy-balanced turbulent Reynolds number, discussed in the previous section, is referred as *second-type* MSV, or MSV-2. We shell elaborate the differences, benefits and disadvantages of MSV-1 and MSV-2 in the following section.

2.3 Application of MSV to Simple Channel Flows (Preliminary Results)

The calculations were performed on the pipe, plane channel and annulus. Computational algorithm is chosen as following:

1. Initial estimation of velocity distribution is calculated as laminar flow, i.e. turbulent viscosity ν_t^l is zero at every point for every scale
2. For every local point turbulent Reynolds number Re_t is calculated with Eq. (26) (in case of MSV-1) or using Eq. (23) and (24) (MSV-2)
3. In those points, where $Re_t < Re_{cr}$, that is *130* in the case of MSV-1 and *8.33* for MSV-2, turbulent viscosity is recalculated with Eq. (27)
4. Using new turbulent viscosity distribution, the velocity profile is recalculated
5. In case of convergence, when the difference between fresh calculated velocity profile does not exceed a given numerical error, calculations stop; otherwise, Step 2 is repeated again.

A computer program in C++ has been developed for PC-Windows platform. It allows calculation of the velocity profiles in simple channels, such as a pipe, plane channel and annular channel. Some visual control features were implemented. Figure 11 shows a sample screen shot of one the program windows. This work is not finished yet and we shell give more details in a future report.

Results of turbulent viscosity calculations are shown in Figs. 12, 13, 14, and 15. Figures 12 and 13 are related to the first-type MSV model, MSV-1. Results calculated for the second-type MSV-2 are shown in Figs. 14 and 15. Calculations for the Reynolds numbers Re=3.2E+4 and Re=1.0E+7 are shown in Figs. 12, 14, and Figs. 13, 15 correspondingly. The upper plots show the turbulent viscosity distributions versus radius while lower plots show the same profiles versus dimensionless distance to the wall y^+. Turbulent viscosity profiles calculated with Reichardt's and three-layers formulas are also shown for comparison.

Brief analysis shows that MSV-2 profiles behave more physically but average magnitude is rather low for higher Reynolds numbers. From the other hand, turbulent viscosity seems to high near the center velocity line in case of the MSV-1 model. However, simple MSV-1 has a very important advantage. It perfectly predicts a friction factor for all Reynolds numbers (except transition area) as shown in Fig. 16. MSV-1 results for friction factor are in a perfect agreement with both famous experimental formula and SuperPipe measurements of Zagarola [25]. MSV-2 significantly underestimates the friction factor for high Reynolds numbers perhaps as a result of underestimation of turbulent viscosity (see Fig. 15 for details).

Dimensionless velocity distributions are shown in Fig. 17 in comparison with SuperPipe experiment. Again, one can see that profiles calculated with MSV-2 are very far from experimental data because of underestimation of friction and, consequently, the friction velocity. Profiles

calculated with MSV-1 are also not shaped very well; even the numerical values are in a good agreement with experimental data.

The flow in plane and annular channels were also calculated. In general, results are very similar to those of the circular tube. Since this report is not final, we show here only one interesting result. Figure 18 shows the calculated position of the maximal velocity line in the annular channels versus internal-to-external diameters ratio. Here, R_{max} is external radius and R_2 is internal radius. Results were calculated with both MSV-1 and MSV-2 and appeared to be the same.

Let us summarize some preliminary conclusions:

- MSV-1 that is based on the very simple definition of the turbulent Reynolds number (see Eq. (26)), predicts very precisely the friction factor in a whole range of Reynolds numbers except transitional ones. The shape of turbulent viscosity distribution is not physical, as well as the shape of velocity profile itself (lower then should be in the central area)
- MSV-2 that is based on more complicated and physically originated relations Eq. (23) and (24) predicts physically acceptable turbulent viscosity profiles but with rather low magnitude for the high Reynolds numbers. The later is the reason why MSV-2 does not predict correctly friction factor and scale of the velocity profile.

If it was possible to combine the physical logic and the right shape of the turbulent viscosity distribution given by MSV-2 and perfect prediction of the friction factor with MSV-1, we would consider the development of the new model of turbulence as completed. However, an additional work is necessary to elaborate the definition of the energy-balanced turbulent Reynolds number. The main direction of the future work is seen as elaboration of the modeling of shear stress in the other direction of the stress tensor.

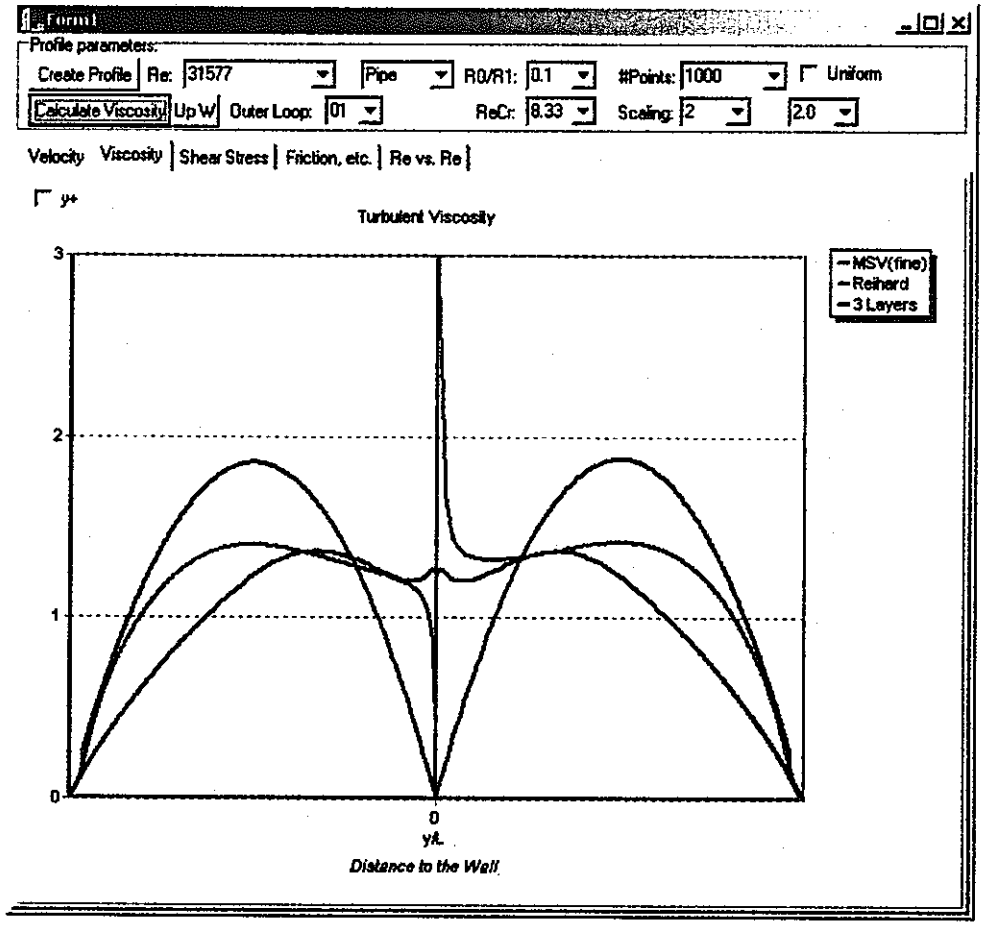

Figure 11. Sample screen shot of calculation program

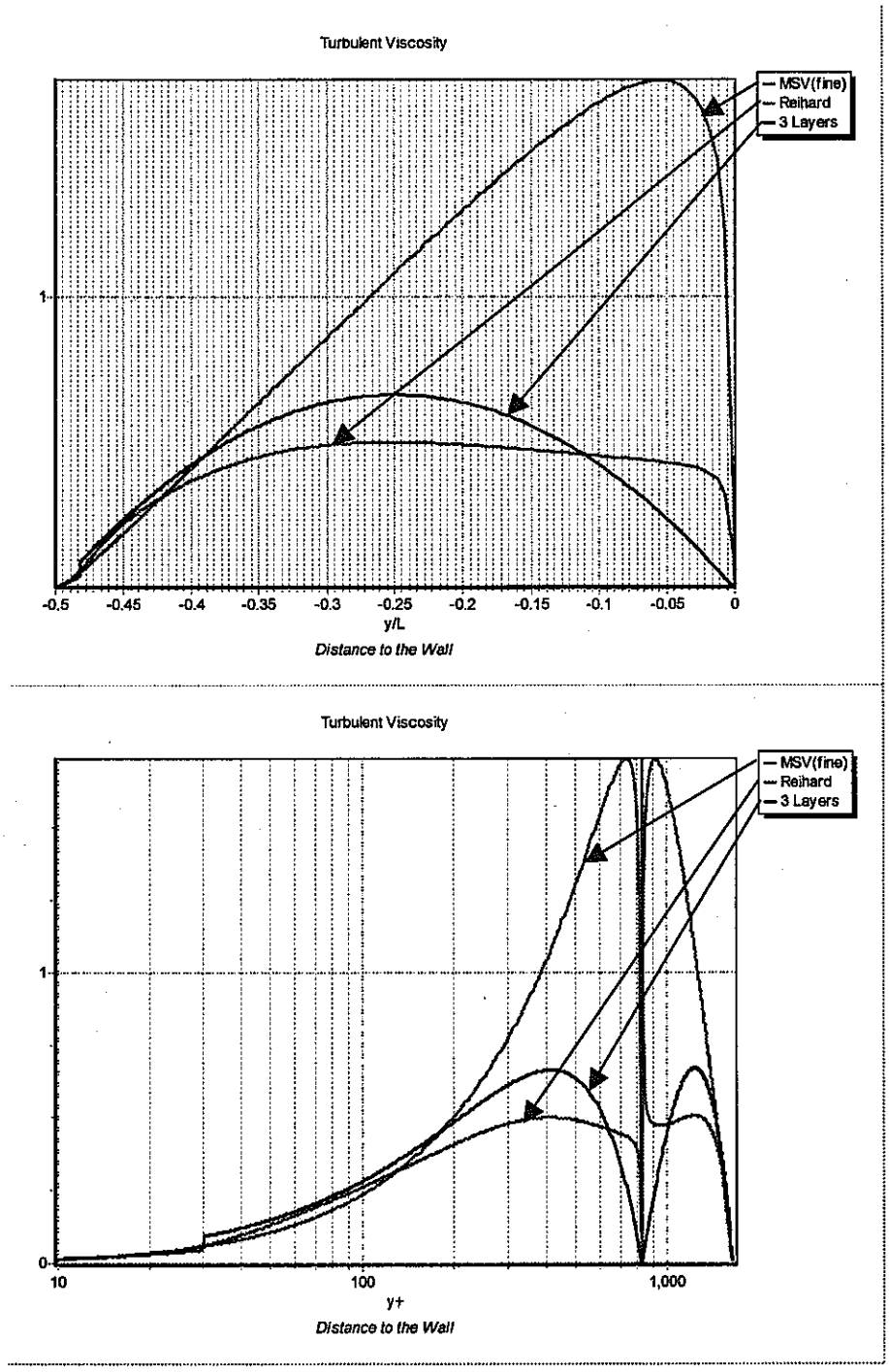

Figure 12. Distribution of eddy diffusivity calculated with first-type MSV model; Re=3.2E+04

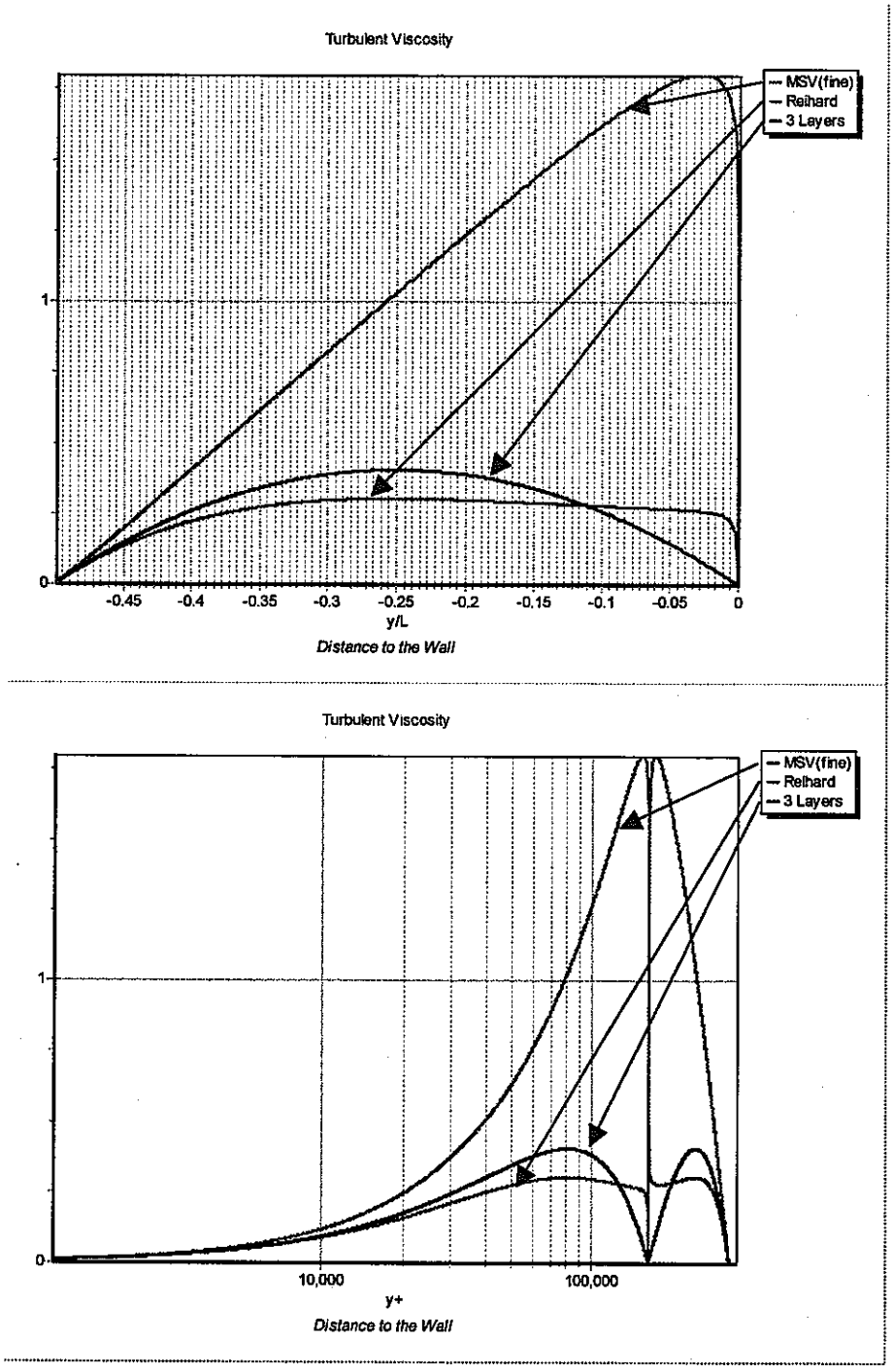

Figure 13. Distribution of eddy diffusivity calculated with first-type MSV model; Re=1.0E+7

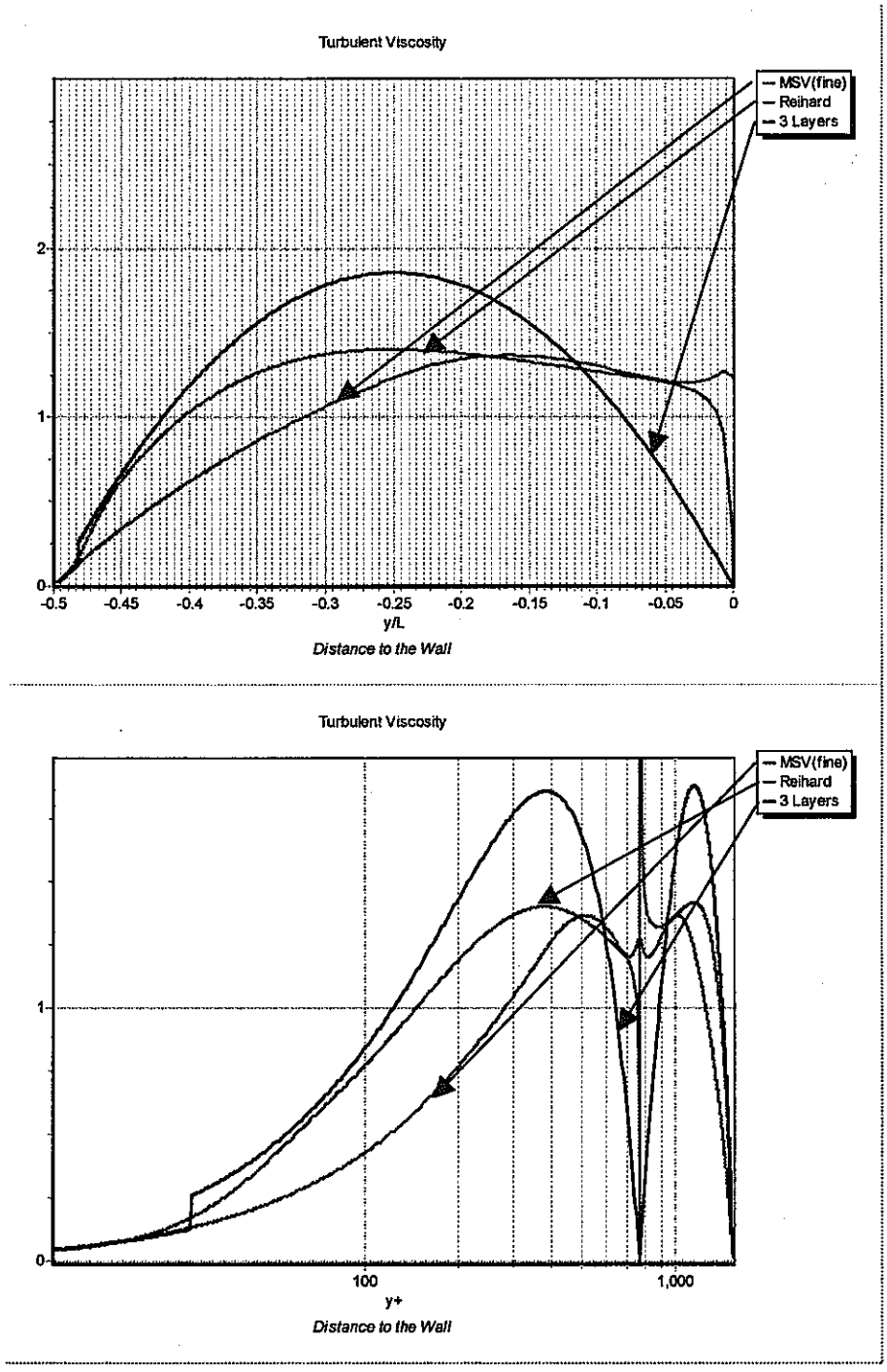

Figure 14. Distribution of eddy diffusivity calculated with second-type MSV model; Re= 3.2E+04

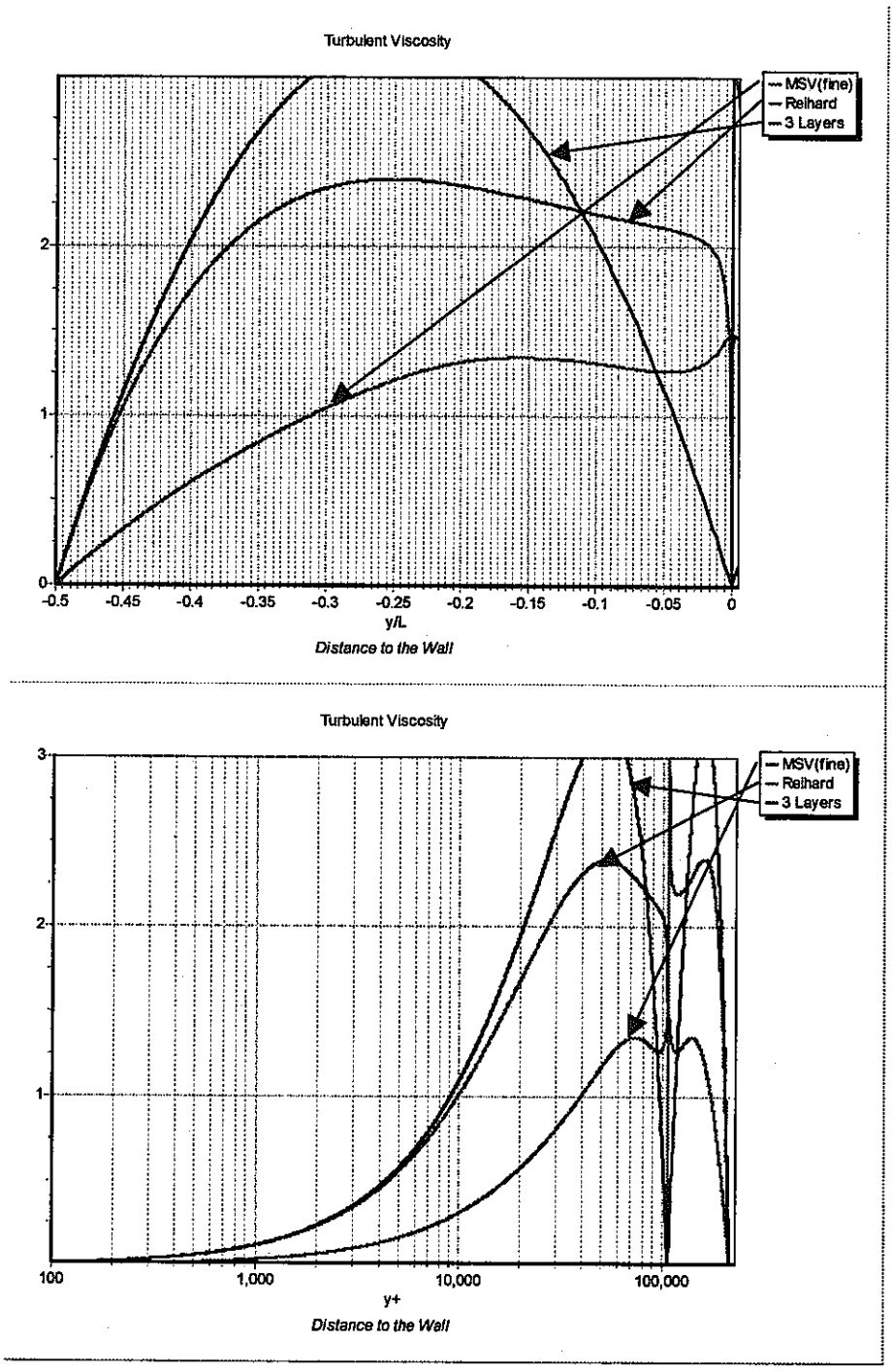

Figure 15. Distribution of eddy diffusivity calculated with second-type MSV model; Re =1.0E+7

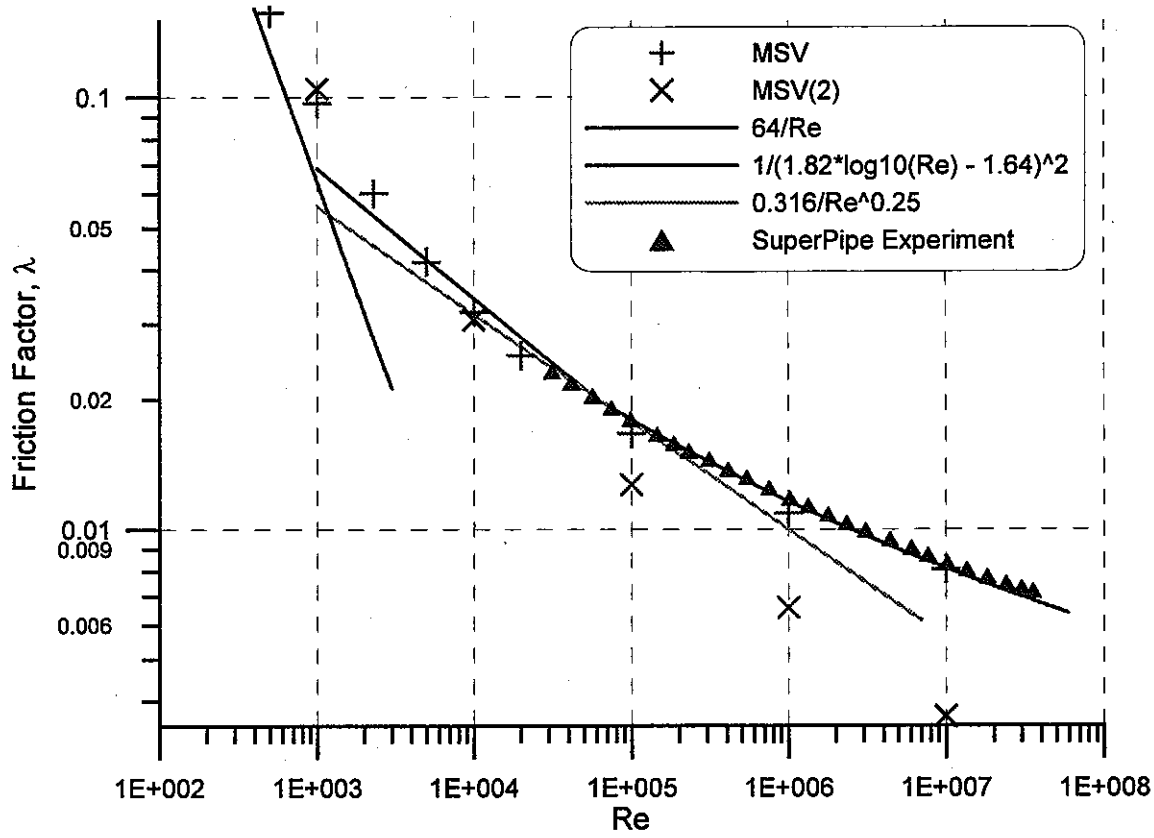

Figure 16. Friction factor calculated with first-type (MSV) and second-type (MSV(2)) models

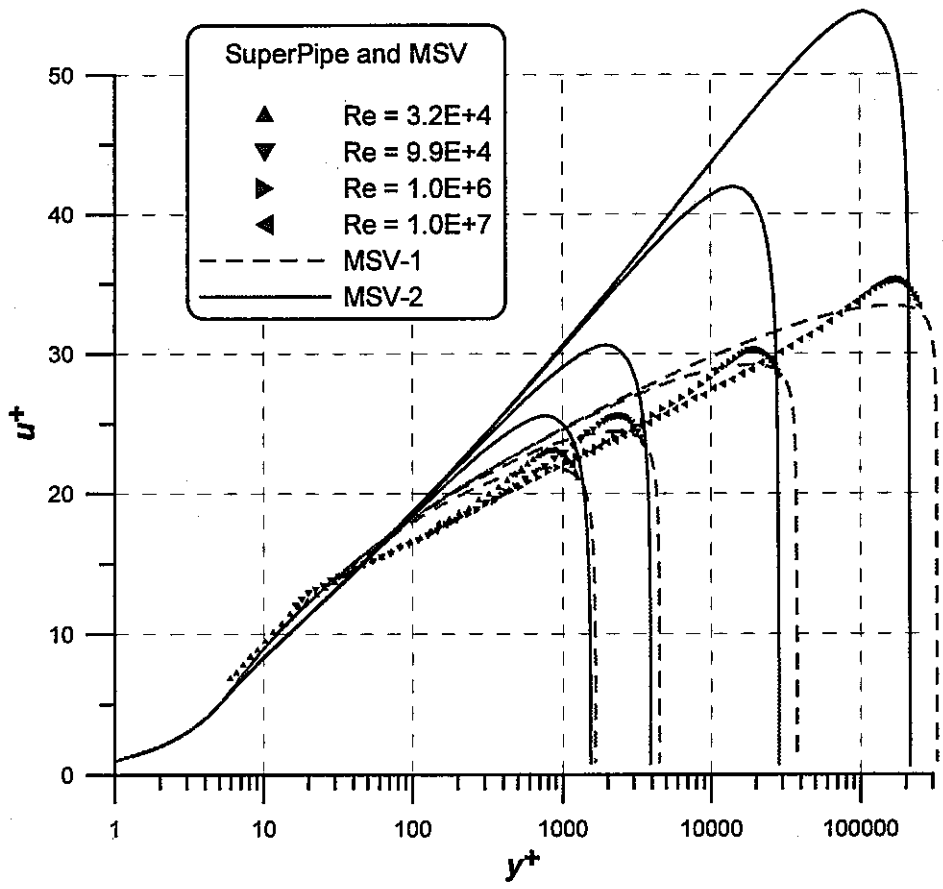

Figure 17. Dimensionless velocity profiles calculated with first-type (MSV-1) and second-type (MSV-2) models in comparison with SuperPipe experiment of Zagarola [25]

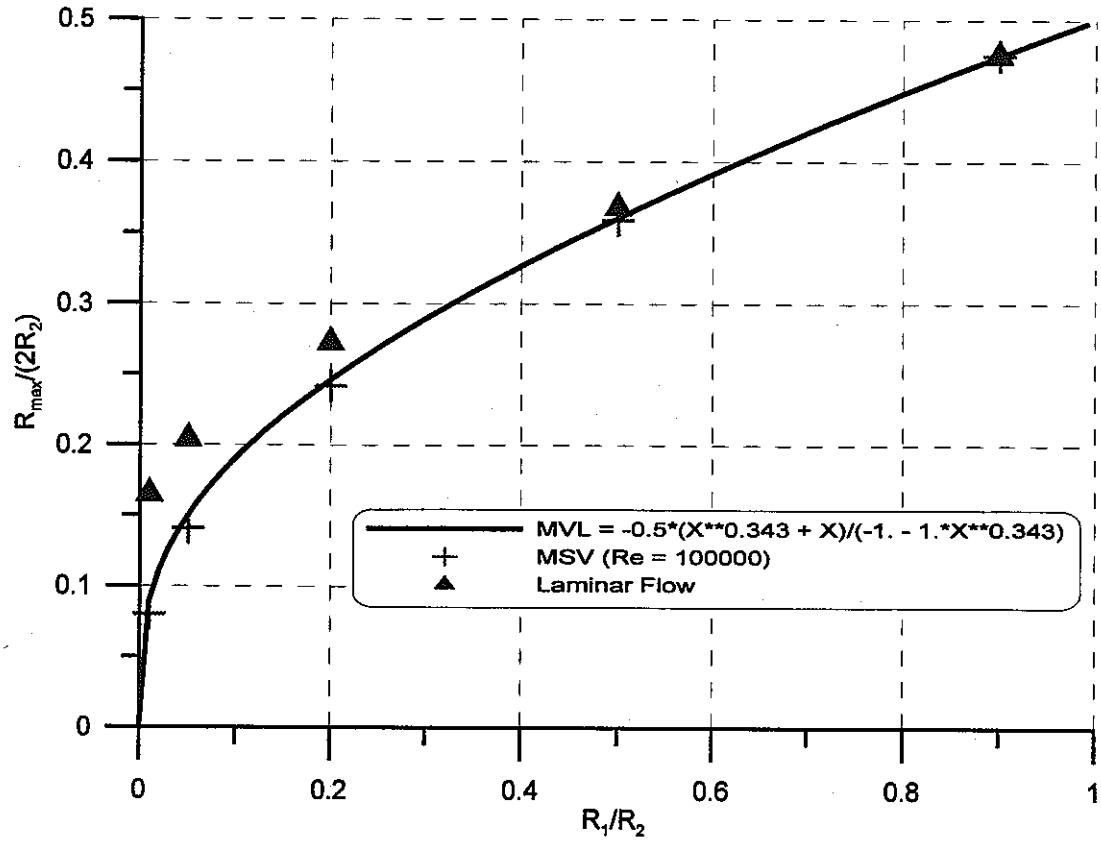

Figure 18. Maximal velocity line in annular channel calculated by first-type MSV model

3. CONCLUSIONS

In this work, preliminary results of Multi-Scale Viscosity (MSV) model have been reported. MSV model can be applied to the fully-developed wall-bounded channels flows. The main idea of MSV is to define an appropriate physical criterion which we call a turbulent Reynolds number, that reflect a level of turbulence within a given area of the channel. In doing so, we assume that the turbulent Reynolds number can never exceed a critical value that is the only experimental parameter used in MSV model. Two different definitions of the turbulent Reynolds number were proposed and investigated:

1. a product of the value of axial velocity deformation for a given scale and generic length of this scale divided by accumulated value of laminar and turbulent viscosity of lower scales
2. a ratio of the difference between total kinetic energy and "flat-profile" kinetic energy to the work of friction forces

The former definition is very simple and logical even it is not derived from basic laws of physics. The later has a clear physical meaning as a balance of two energies: i) energy necessary to change velocity profile to flat, minimizing the energy loss due to momentum transport and ii) work of friction forces.

Both definitions of the turbulent Reynolds number above have been examined on the basic shape flows: a circular pipe, a plane channel and an annular channel. The results of calculation shows that the first model can very accurate predict a friction factor that is an integral conservative parameter. However, it cannot predict a right physical shape of the turbulent viscosity profile. From the other hand, the second model predicts physically correct distribution of turbulent viscosity but the magnitude is underestimated for high Reynolds numbers. As a result, the second model underestimates the friction factor as well.

A very attractive feature of MSV, that it is capable to predict a turbulent flow in complicated shapes, like a fuel assemble of the nuclear reactor. In this work, we declare that MSV can been applied to wall-bounded flows. However, there are some reasons to believe that MSV can also work in more general turbulent flow, such as a boundary layer flow.

Possible ways of the MSV model improvements are discussed. New results will be presented in a future final report.

4. ACKNOWLEDGEMENT

The author of this work would like to thank Prof. P.L. Kirillov of IPPE (Institute of Physics and Power Engineering, Obninsk, Russia) for very valuable discussion that helped to formulate the concept of the turbulent Reynolds number.

REFERENCES

1. L. Prandtl, Uber Die Ausgebildete Turbulenz (On the fully developed turbulence), *ZAMM (Journal of Applied Mathematics and Mechanics)* Vol. 5 pp.136-139 (1925).
2. C.-J. Chen, S.-Y. Jaw, *Fundamentals of Turbulence Modeling*, Taylor & Francis, New York (1989).
3. Y.A. Hassan, J.M. Pruitt and D.A. Steininger, A Perspective on Large Eddy Simulation of Problems in the Nuclear Industry, *Nuclear Technology*, Vol.112, pp. 324-330 (1995).
4. N.I. Buleev, Theoretical Model of Turbulent Exchange in Fluid Flow and Heat-Transfer Problems, in *Heat-Transfer*, USSR Academy of Sci. pp.64-98 (in Russian) (1962); also in Proc. Of Third Intl. Conf. On Peaceful Uses of Atomic Energy, N.Y., Vol.8, pp.305-315 (1965).
5. N.I. Buleev, Further Development of Space Model of Turbulent Exchange in Non-Compressible Flow, in *Near-Wall Turbulent Flow*, SO-AN USSR, part. I, pp.51-79 (in Russian) (1975).
6. W. Pfeninger, Transition Experiments in the Inlet Length of Tubes at High Reynolds Numbers *Boundary Layer and Flow Control* (ed. G.V. Lachman), Pergamon, pp.970-980 (1961)
7. I. Wygnanski, F.H. Champagne, On Transition In a Pipe. Part 1. The origin of Puffs and Slugs and the Flow in a Turbulent Slug, *Journal of Fluid Mechanics*, Vol. 59, pp.281-335 (1973).
8. I. Wygnanski, M. Sokolov and D. Friedman, On Transition In a Pipe. Part 2. The Equilibrium Puff, *Journal of Fluid Mechanics*, Vol. 69, pp.283-304 (1975).
9. H. Eckelman, The Structure of the Viscous Sublayer and the Adjacent Wall Region in a Turbulent Channel Flow, *Journal of Fluid Mechanics*, Vol. 65, pp.439-459 (1974).
10. H.-P. Kreplin and H. Eckelman, Behavior of the Three Fluctuating Velocity Components In the Wall Region Of a Turbulent Channel Flow, *Physics of Fluids*, Vol. 22, pp.1233-1239 (1979).
11. L.C. Thomas, A Turbulent Burst Model of Wall Turbulence For Two-Dimensional Turbulent Boundary Layer Flow, *Int. Journal of Heat and Mass Transfer*, Vol. 25, No 8, pp.1127-1136 (1982).
12. E. Alp and A.B. Strong, Measurements of Characteristic Time Scales of the Turbulent Boundary Layer With Mass Transfer, *Int. Journal of Heat and Mass Transfer*, Vol. 24, No 3, pp.521-531 (1981).
13. P.L. Kirillov, On Influence of Thermal-Physics Properties of Wall on Heat-Transfer in Turbulent Flow, Ingenerno-Physichesky Journal, Vol. L, No 3, pp.501-512, (1986) (in Russian).
14. J. Mizushima and Y. Shiotani, Structural Instability of the Bifurcation Diagram for Two-Dimensional Flow in a Channel With a Sudden Expansion, *Journal of Fluid Mechanics*, Vol. 420, pp.131-145 (2000).
15. P. Bradshaw, A Note On "Critical Roughness Height" and "Transitional Roughness", *Physics of Fluids*, Vol. 12, pp.1611-1614 (2000).
16. J. Nikuradse, Laws of flow I rough pipes, VDI Forschungsheft, No. 361 (1933): translated as British ARC paper 986 (1933).
17. S. Eliahou, A. Tumin and I. Wygnanski, Laminar-Turbulent Transition In Poiseuille Flow Subjected to Periodic Perturbations Emanating From the Wall, *Journal of Fluid Mechanics*, Vol. 361, pp.333-349 (1998).

18. G. Han, A. Tumin and I. Wygnanski, Laminar-Turbulent Transition in Poiseuille Pipe Flow Subjected to Periodic Perturbation Emanating from the wall. Part 2. Late Stage of transition, *Journal of Fluid Mechanics*, Vol. 419, pp.1-27 (2000).

19. J.-Y. Vincont, S. Simoens, M. Ayrault, J.M. Wallace, Passive Scalar Dispersion in a Turbulent Boundary Layer From a Line Source At the Wall and Downstream of an Obstacle, *Journal of Fluid Mechanics*, Vol. 424, pp.127-167 (2000).

20. P. Andersson, L. Brandt, A. Bottaro, D.S. Henningson, On the Breackdown of Boundary Layer Streaks, *Journal of Fluid Mechanics*, Vol. 428, pp.29-60 (2001).

21. R.J. Adrian, C.D. Meinhart and C.D. Tomkins, Vortex Organization in the Outer Region of the Turbulent Boundary Layer, *Journal of Fluid Mechanics*, Vol. 422, pp.1-54 (2000).

22. A.V. Johansson and P.H. Alfredsson, On the Structure of Turbulent Channel Flow, *Journal of Fluid Mechanics*, Vol. 122, pp.295-314 (1982).

23. J. Kim, P. Moin and R.T. Moser, Turbulence Statistics in Fully Developed Channel Flow at Low Reynolds Number, *Journal of Fluid Mechanics*, Vol. 177, pp.133-166 (1987).

24. P.R. Spalart, Direct Numerical Simulation of a Turbulent Boundary Layer up to $Re_\theta = 1410$, *Journal of Fluid Mechanics*, Vol. 187, pp.61-98 (1988).

25. M.V. Zagarola, *Mean Flow Scaling of Turbulent Pipe Flow*, Ph.D. Thesis, Department of Mechanical and Aerospace Engineering, Princeton University, (1996).

26. M.V. Zagarola and A.J. Smits, Mean-Flow Scaling of Turbulent Pipe Flow, *Journal of Fluid Mechanics*, Vol. 373, pp.33-79 (1998).

27. H. Reichardt, Vollstandige Darstellung der turbulenten beschwindigkeitsverteilung in glatten Zeitungen, *Zeitschrift für angen. Math. und Mechanik*, Bd. 31, No.7, pp.208-219

28. K.R. Sreenivasan, The Turbulent Boundary Layer, *Frontiers in Experimental Fluid Mechanics*, Vol. 46, pp.159-209 (1989).

29. H.H. Fernholz and P.J. Finley, The Incompressible Zero-Pressure-Gradient Turbulent Boundary Layer: An Assessment of the Data, *Progress Aerospace Science*, Vol. 32, pp.25-311 (1996).

30. D.B. DeGraff and J.K. Eaton, Reynolds-Number Scaling of the Flat-Plate Turbulent Boundary Layer, *Journal of Fluid Mechanics*, Vol. 422, pp.319-346 (2000).

31. G.I. Barenblatt, V.M Prostokishin, Scaling Laws for Fully Developed Turbulent Shear Flows. Part 1. Basic Hypotheses and Analysis, *Journal of Fluid Mechanics*, Vol. 248, pp.513-520 (1993).

32. G.I. Barenblatt, V.M Prostokishin, Scaling Laws for Fully Developed Turbulent Shear Flows. Part 2. Processing of Experimental data, *Journal of Fluid Mechanics*, Vol. 248, pp.521-529 (1993).

33. G.I. Barenblatt, *Scaling, Self-Similarity, and Intermediate Asymptotics*, Cambridge University Press (1996).

34. M. Wosnik, L. Castilio and W.K. George, A Theory for Turbulent Pipe and Channel Flows, *Journal of Fluid Mechanics*, Vol. 421, pp.115-145 (2000).

35. H. Schlichting, *Grenzschicht-Theorie*, G. Braun, (1968).

36. S.C. Kassinos, W.C. Reynolds, M.M. Rogers, One-Point Turbulence Structure Tensors, *Journal of Fluid Mechanics*, Vol. 428, pp.213-248 (2001).